Available online at www.sciencedirect.com

ScienceDirect

Advances in Space Research 64 (2019) 1948–1967

ADVANCES IN SPACE RESEARCH (a COSPAR publication)

www.elsevier.com/locate/asr

New techniques for retrieving the [O(^{3}P)], [O_3] and [CO_2] altitude profiles from dayglow oxygen emissions: Uncertainty analysis by the Monte Carlo method

Valentine Yankovsky *, Ekaterina Vorobeva, Rada Manuilova

Atmospheric Physics Department, Saint Petersburg State University, 7/9 Universitetskaya nab., Saint Petersburg 199034, Russia

Received 8 March 2019; received in revised form 15 June 2019; accepted 16 July 2019
Available online 24 July 2019

Abstract

This study presents methods for retrieving the altitude profiles of atomic oxygen, [O(^{3}P)], ozone, [O_3], and carbon dioxide, [CO_2], concentrations in the daytime mesosphere and lower thermosphere (MLT) in the framework of the YM2011 model of the electronic-vibrational oxygen kinetics. The emissions of singlet oxygen molecules $O_2(b^1\Sigma_g^+, v \leq 2)$, $O_2(a^1\Delta_g, v = 0)$ and the O(^{1}D) atom are used as proxy of the [O(^{3}P)], [O_3] and [CO_2]. For all the proposed techniques, we compare the uncertainty values of the retrieved [O(^{3}P)], [O_3] and [CO_2], obtained by the Monte Carlo method, with estimations obtained by the sensitivity analysis method in the earlier works. For all the above mentioned methods for retrieving the [O(^{3}P)], [O_3] and [CO_2] profiles, we obtained analytical expressions that include the concentrations of excited substances considered as proxies. In addition, the optimal altitude ranges for using these remote sensing methods were determined based on the results of numerical experiments by the Monte Carlo method.

Keywords: Remote sensing; Mesosphere and low thermosphere; Atomic and molecular oxygen emissions; Carbon dioxide; Uncertainty analysis; Monte-Carlo method

1. Introduction

In recent decades, various methods for retrieving the altitude profiles of atomic oxygen, [O(^{3}P)], ozone, [O_3], and carbon dioxide, [CO_2], concentrations in the mesosphere and lower thermosphere (MLT) from observations of the intensity of oxygen emissions have been developed (Witasse et al., 1999; Mlynczak et al., 2001; Marsh et al., 2002; Yankovsky and Manuilova, 2006; Hedin et al., 2009; Gattinger et al., 2010; Yee et al., 2012; Hecht et al., 2015; Yankovsky et al., 2016; Martyshenko and Yankovsky, 2017; Yankovsky and Manuilova, 2018; Wu et al., 2018). These atmospheric components play a key role in the energy balance of the atmosphere at MLT altitudes. The most accurate methods for retrieving the altitude profiles of the components under consideration are associated with the absorption of radiation from stars or the Sun. However, these methods work only at twilight and cannot track diurnal variations in the altitude profiles of the concentration of these components. Therefore, methods based on photochemical modeling of atmospheric processes are becoming one of the main sources of information on the composition of the atmosphere during the day.

This principle is the basis of a number of well-known satellite experiments: TIMED-SABER (Thermosphere, Ionosphere, Mesosphere, Energetics and Dynamics – Sounding of the Atmosphere using a Broadband Emission Radiometry) and ODIN in 1.27 μm channel and HRDI

* Corresponding author.
E-mail addresses: vyankovsky@gmail.com, valentine.yankovsky@spbu.ru (V. Yankovsky).

https://doi.org/10.1016/j.asr.2019.07.020
0273-1177/

(High Resolution Doppler Imager) in 0.762 μm channel (Khabibrakhmanov et al., 2002; Marsh et al., 2002; Smith et al., 2013). The ideology of these experiments is based on the solution of the forward problem, namely, the theoretical calculation of the excited atmospheric component concentration altitude profile, which is compared with the measurement results. To interpret the experiment, it is necessary to solve the inverse problem of retrieving the target component concentration from measuring the intensity of the corresponding emission in the framework of basic photochemical model. The classic task of this type is the algorithm for retrieval of the $[O_3]$ altitude profile in MLT in daytime conditions from observing the altitude profile of the volume emission rate (VER) of the IR Atmospheric oxygen band centered at 1.27 μm (Llewellyn and Witt, 1977, Evans et al., 1988; etc.).

Yankovsky et al. (Yankovsky et al., 2016, Yankovsky and Manuilova, 2018) proposed five proxies for retrieval of the $[O(^3P)]$, $[O_3]$ and $[CO_2]$ altitude profiles. This study presents methods for retrieval of the $[O(^3P)]$, $[O_3]$ and $[CO_2]$ altitude profiles in the daytime MLT using the emissions of five proposed proxies, $O_2(b^1\Sigma_g^+,\ v \le 2)$, $O_2(a^1\Delta_g,\ v = 0)$ and $O(^1D)$, within the framework of the YM2011 model of the electronic-vibrational oxygen kinetics (Yankovsky et al., 2011). The model was developed for the daytime conditions of the mesosphere and lower thermosphere, and takes into account the energy transfer, as well as the complex of collisional reactions and radiative deexcitation of all excited substances considered as proxies. The YM2011 model allows not only theoretically simulating the intensity of emissions of singlet oxygen molecules $O_2(b^1\Sigma_g^+,\ v \le 2)$, $O_2(a^1\Delta_g,\ v = 0)$ and $O(^1D)$ atom in the MLT, but also allows the development of new techniques to retrieve the altitude profiles of the $[O(^3P)]$, $[O_3]$ and $[CO_2]$. Each of the proposed methods is an analytical expression depending not only on proxy concentrations, but also on other parameters of the model, such as concentrations of main atmospheric components, kinetic temperature, rates of photoexcitation processes, rate coefficients of collisional processes of energy exchange, quantum yields of reaction products, and also on the measured volume emission rates. All these parameters have experimentally measured errors and have an independent impact on the final result of retrieval of the target component altitude profile (Yankovsky et al., 2016, Yankovsky and Manuilova, 2018).

Thus, there are four sources of uncertainty in the task of retrieving the altitude profiles of the target component concentrations, namely, the errors of: the parameters of the composition of the background atmosphere; the values of the rate coefficients and quantum yields of the products of photochemical reactions; the measurements of intensities of atmospheric emission and calculations of the volume emission rates; calculations of the rates of excitation processes (photoprocesses in the Hartley and Huggins bands, the Schumann-Runge continuum, H Lyman-α line, and resonant excitation processes) based on spectral composition of solar radiation in the UV and visible regions of the spectrum.

The errors of the calculated rates of excitation processes (Section 4) and the background composition of the atmosphere have insignificant values of the order of 1% (Picone et al., 2002; SORCE, 2003; Gao et al., 2015; etc.). At the same time, the values of the reaction rate coefficients have errors from a percent to several tens of percent, and it is difficult to a priori estimate the magnitude of the contribution of these errors to the final result of retrieval (Yankovsky et al., 2016).

Thus, at solving both forward and inverse problems, we deal with a set of parameters, each of which can randomly vary within its error and make its own contribution to the relative uncertainty of the target component concentration. An effective method for solving such problems is the Monte Carlo method, which allows to take into account a large number of randomly varying model parameters and, accordingly, provides a realistic estimate of the uncertainty of the target component concentration altitude profile retrieval.

In (Mlynczak et al., 1993; von Savigny et al., 2005; Jonsson, 2006; Christensen et al., 2012; Burrows et al., 2013; etc.) the sensitivity analysis of complex photochemical systems was carried out by varying the selected parameters with fixed values of the other parameters (sometimes this approach is called the impact-method). As shown by Yankovsky et al. (2016), this approach for analyzing the sensitivity of complex photochemical systems is not complete. In this study, for comparison with the results of a numerical experiment using the Monte Carlo method, we use the sensitivity analysis from (Yankovsky et al., 2016) that takes into account all parameters without exception. In the present work, we applied the Monte Carlo method to estimate the uncertainties of retrieval of the $[O(^3P)]$, $[O_3]$ and $[CO_2]$ altitude profiles from the intensities of oxygen emissions, and based on the obtained estimates, we determined the optimal altitude intervals for retrieving the altitude profiles of the target components concentration. In addition, we compare the results obtained by the Monte Carlo method with the results of the sensitivity analysis.

The structure of the work is as follows. Section 2 presents the photochemistry of the electronically-vibrationally excited oxygen components in the daytime MLT within the framework of the YM2011 model, and presents the recalculated Einstein coefficients for transitions in the O_2 Atmospheric bands.

In Section 3 we present the theoretical foundations of two ways of estimating the uncertainty of the photochemical system, namely, the Monte Carlo method and the sensitivity analysis.

In Section 4, we estimated the uncertainties of solving the forward problems of calculating the altitude profiles of the excited components $[O(^1D)]$, $[O_2(b^1\Sigma_g^+,\ v \le 2)]$ and

[$O_2(a^1\Delta_g, v = 0)$] and made a comparison of the estimates obtained by the Monte Carlo method and the estimates from the sensitivity analysis.

In Section 5, we present the methods of retrieval of the [O(^{3}P)], [O_3] and [CO_2] altitude profiles using the excited oxygen molecules $O_2(b^1\Sigma_g^+, v \leq 2)$, $O_2(a^1\Delta_g, v = 0)$ and O(^{1}D) atom as proxies and compare estimates of the uncertainty of solving the inverse problems obtained by the Monte Carlo method, and the estimates from the sensitivity analysis.

In Section 6 we discuss the most important results of the study.

2. Photochemistry of excited oxygen components in the daytime MLT

The study deals with the photochemistry of oxygen components in the calm daytime atmosphere under typical conditions for equatorial and middle latitudes. It should be emphasized that for radiation formed by transitions from electronically-vibrationally excited levels of molecular oxygen, the local thermodynamic equilibrium (LTE) is broken. The reason for this is the presence of the constant sources of excitation of these levels, such as absorption of solar radiation, energy transfer from an O(^{1}D) atom and others. In addition, the energy difference between the excited vibrational levels of the oxygen molecule is of the order of 0.19 eV (about 2200 K), which is an order of magnitude greater than the gas kinetic temperature.

The mechanisms of formation and quenching of electronically-vibrationally excited levels of the oxygen molecule were considered in detail in Yankovsky and Manuilova (2006), Yankovsky and Babaev (2011), Yankovsky et al. (2011, 2016), Martyshenko and Yankovsky (2017), Yankovsky and Manuilova (2018). It was shown that the populations of these levels depend not only on the [O_2] and [N_2] altitude profiles but also on the [O(^{3}P)], [O_3] and [CO_2] altitude profiles. The excited levels of molecular oxygen are the sources of atmospheric emissions in the near IR region of the spectrum. The scheme of excited oxygen levels is shown in Fig. 1, with the location of the levels scaled in energy units (eV on the left or cm^{-1} on the right).

The excitation of the O(^{1}D) atom and the singlet levels of the oxygen molecule requires an energy of about 2 eV and less. In daytime conditions, the source of this energy is the photolysis of O_2 in the Schumann-Runge continuum (SRC) and the H Lyman-α line (Lyα), and O_3 in the Hartley and Huggins bands (HHB) (see Fig. 1).

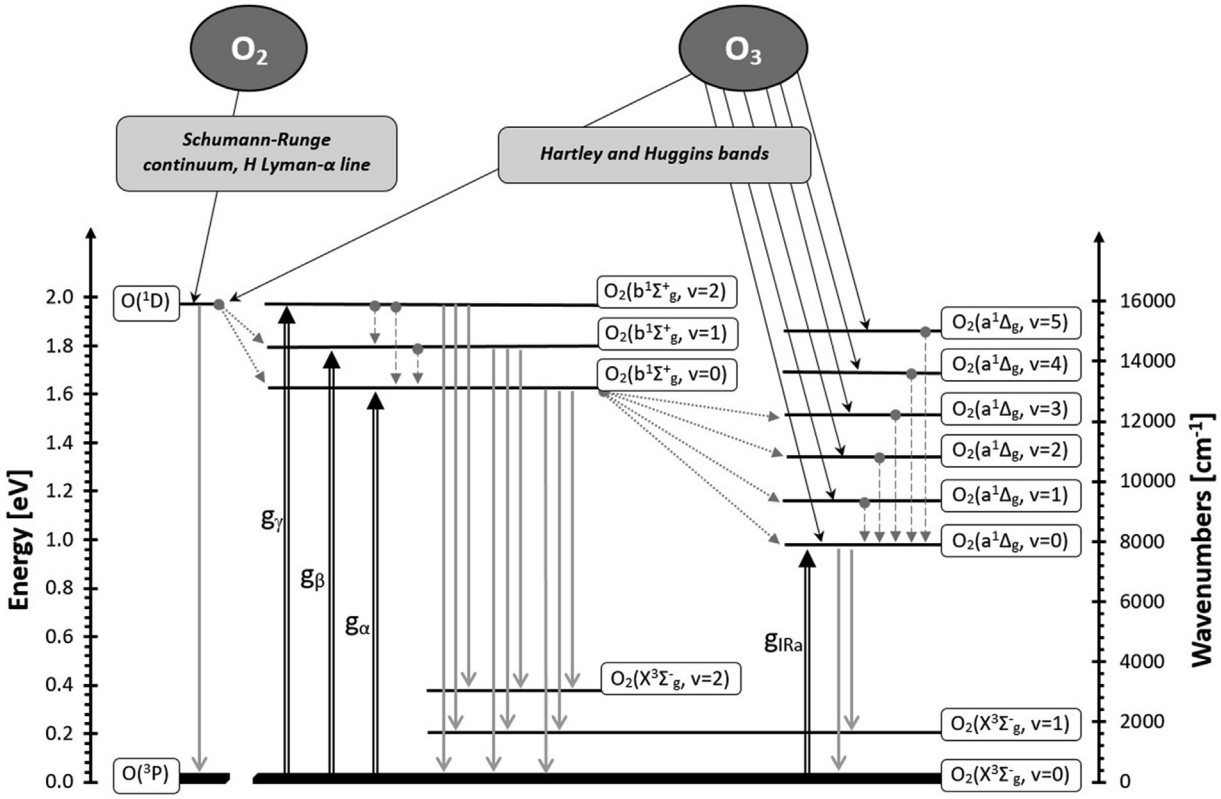

Fig. 1. Scheme of kinetics of 10 excited levels, based on the YM2011 model: O(^{1}D), three $O_2(b^1\Sigma_g^+, v = 0–2)$ levels, and six $O_2(a^1\Delta_g, v = 0–5)$ levels. Solid lines with arrows designate the processes of O_2 photodissociation in Schumann-Runge continuum and H Lyman - α line and O_3 photolysis in Hartley and Huggins bands. Double vertical lines with the arrows pointed upwards designate the processes of solar radiation absorption in the 762 nm (g_α), 688 nm (g_β), 629 nm (g_γ) and in the 1.27 μm (g_{IRa}) bands. Dotted lines with arrows present energy transfer from O(^{1}D) to the $O_2(b^1\Sigma_g^+, v = 0, 1)$ and from $O_2(b^1\Sigma_g^+, v = 0)$ to $O_2(a^1\Delta_g, v = 0–3)$ at collisional quenching. Dashed vertical lines with arrows pointed down stand for collisional V-V transitions. Solid vertical grey lines with arrows pointed down designate the processes of radiative emissions from electronic-vibrational levels of O_2 molecule and from excited atom O(^{1}D).

There is another source of excitation of the singlet and triplet levels of the oxygen molecule – the association of oxygen atoms in the triple reaction (Barth's mechanism) (Grygalashvyly et al., 2019). While at night this mechanism dominates in the altitude range of 90–103 km, during the daytime its contribution compared to photolysis of O_2 and O_3 varies from fractions of a percent to a few percent according to estimates by (Wu et al., 2018, Yee et al., 2012, etc.). Therefore, this mechanism is not considered in this paper.

Fig. 1 shows the scheme of energy transfer between the products of O_3 and O_2 photolysis leading to the formation of electronically-vibrationally excited molecules in the $O_2(b^1\Sigma_g^+, v \le 2)$ and $O_2(a^1\Delta_g, v \le 5)$ states, as well as the O (^{1}D) atom. The traditional channel of the $O_2(a^1\Delta_g, v)$ excitation is O_3 photolysis in the singlet channel. The alternative channel of the $O_2(a^1\Delta_g, v = 0)$ excitation is multistage. As can be seen from the scheme, the levels $O_2(b^1\Sigma_g^+ v = 0, 1)$ are excited due to the energy transfer from the O(^{1}D) atom formed during the photolysis of O_2 and O_3. Further, the energy of the level $O_2(b^1\Sigma_g^+, v = 0)$ goes to the excitation of the levels $O_2(a^1\Delta_g, v = 0–3)$ with subsequent collisional relaxation to the level $O_2(a^1\Delta_g, v = 0)$. The processes of exciting and quenching of all these levels are described by more than seventy photochemical reactions. In Yankovsky et al. (2016), Yankovsky and Manuilova (2018) within the framework of the YM2011 model, we presented the databases on the values of the rate coefficients and quantum yields of the reaction products with their errors.

In Yankovsky et al. (2016), we presented the complete kinetic equations for populations of ten excited levels (O (^{1}D), $O_2(b^1\Sigma_g^+, v = 0–2)$, $O_2(a^1\Delta_g, v = 0–5)$). In the present study we used these equations to solve forward and inverse problems.

2.1. Notations

Further, for a compact representation of the equations presented in the work, the following abbreviated notations will be used:

(a) Brief notation of levels: $O_2(b^1\Sigma_g^+, v) = O_2(b, v)$, $O_2(a^1\Delta_g, v) = O_2(a, v)$, $O_2(X^3\Sigma_g^-, v) = O_2(X, v)$.
(b) $k(A^*; B)$ is the rate coefficient of bimolecular reaction $A^* + B \to C^{**} + D$ in units of cm^3s^{-1}.
(c) For the quantum yield value of each product C^{**} of reaction $A^* + B \to C^{**} + D$, we use the designation $F(A^* \to C^{**}; B)$, since in most reactions there are several channels of formation of the product C^{**} depending on collision partner B.
(d) J_{HHB} – the O_3 photolysis rate in Hartley and Huggins bands. $J_{SRC,}$ and $J_{Ly\alpha} - O_2$ photolysis rate in the Schumann-Runge continuum and in the line of H Lyman-α, respectively.
(e) The most often used in the model YM2011 notations of the quantum yields of the reaction products $F(A^* \to C^{**}; B)$ are redesignated to reduce the writing of the formulas:

$$F(Ly\alpha) = F(O_2 \to O(^1D); Ly\alpha)$$
$$F(HHB) = F(O_3 \to O(^1D); HHB)$$
$$F(HHB \to a, v) = F(O_3 \to O_2(a, v); HHB)$$
$$\psi_1 = F(O(^1D) \to O_2(b, v = 1); O_2)$$
$$\psi_0 = F(O(^1D) \to O_2(b, v = 0); O_2)$$
$$\psi_{b,2\to b,v} = F(O_2(b, v = 2) \to O_2(b, v); O(^1P))$$
$$\psi^M_{b,0\to a,v} = F(O_2(b, v = 0) \to O_2(a, v); M)$$

(f) The rates of resonant absorption of solar radiation by O_2 molecules in the bands with centers of 762 nm, 688 nm, 629 nm and 1.27 μm are denoted as g_α, g_β, g_γ and g_{IRa}, respectively.
(g) The amplitude of the relative error of the value of any parameter z of the model is denoted as ξ_z. We use experimentally determined values of the relative errors of the parameters $\xi_z = \Delta z / z$, where Δz is the absolute value of the error of the parameter z. All these constants are currently known and are given in the Supplementary Material.

2.2. Einstein coefficients and radiative lifetime

Optical transitions $O_2(b^1\Sigma_g^+, v) \to O_2(X^3\Sigma_g^-, v)$ and $O_2(a^1\Delta_g, v) \to O_2(X^3\Sigma_g^-, v)$ form a system of O_2 Atmospheric bands in the near infrared spectrum. Most of these emissions have actually been observed in the atmosphere for several decades (Torr and Torr, 1985). The concentration of molecules in the excited state is equal to the ratio of volume emission rate (VER) to the Einstein coefficient for the corresponding transition, A_E. Therefore, Einstein coefficients of the corresponding optical transitions are necessary for retrieving the concentrations of the excited oxygen molecules $O_2(b^1\Sigma_g^+, v' \ge 0)$ and $O_2(a^1\Delta_g, v' \ge 0)$ from the measured values of VER in the O_2 Atmospheric bands.

In addition, Einstein coefficients are related to the radiative deexcitation. The radiative lifetime of $O_2(b^1\Sigma_g^+, v')$ levels is

$$\tau_{O_2(b,v')} = \frac{1}{\sum_{v''} A_{O_2(b,v'\to X,v'')} + \sum_{v''} A_{O_2(b,v'\to a,v'')}}, \quad (1)$$

which takes into account transitions in Atmospheric band and Noxon band to all lower levels.

The radiative lifetime of $O_2(a^1\Delta_g, v')$ levels is

$$\tau_{O_2(a,v')} = \frac{1}{\sum_{v''} A_{O_2(a,v'\to X,v'')}}, \quad (2)$$

and takes into account transitions in IR Atmospheric band.

Currently, there is no complete and uniform database of Einstein coefficients for transitions from the electronic-vibrationally excited $O_2(b^1\Sigma_g^+, v' \ge 0)$ and $O_2(a^1\Delta_g, v' \ge 0)$ levels. For example, there are next values of $O_2(b^1\Sigma_g^+, v' = 0)$ radiative lifetime: 13.2 s (Slanger and Copeland,

2003), 10.8 s (Yee et al., 2012), 12.0 s (Slanger et al., 2017), etc. This scatter of data does not allow a sufficient assessment of the radiative deexcitation in modeling of photochemical processes. In this study, we tried to clarify this issue.

Newly calculated Frank-Condon coefficient values for transitions in three O_2 band systems, namely, Atmospheric, $O_2(b^1\Sigma_g^+,\ v' \le 10 \rightarrow X^3\Sigma_g^-,\ v'' \le 35)$, Noxon, $O_2(b^1\Sigma_g^+,\ v' \le 10 \rightarrow a^1\Delta_g,\ v'' \le 15)$, and IR Atmospheric, $O_2(a^1\Delta_g,\ v' \le 10 \rightarrow X^3\Sigma_g^-,\ v'' \le 35)$, were recently published in Yu et al. (2014). Using this data, we calculated the Einstein coefficients for emission transitions in these bands by the method of (Kassi et al., 2005; Kuznetsova et al., 1980) (see Appendix A). We found out that the contribution of radiative deexcitation in the Noxon band is 1.7% of the total radiative lifetime of $O_2(b^1\Sigma_g^+,\ v')$ level.

In this study (Fig. 1), it is necessary to know the Einstein coefficients for the transitions from $O_2(b^1\Sigma_g^+,\ v \le 2)$ and $O_2(a^1\Delta_g,\ v \le 5)$ levels to the $O_2(X^3\Sigma_g^-,\ v \le 2)$ levels, as well as the radiative lifetimes of these levels (Table 1).

3. Two ways to determine the uncertainty of the photochemical model

3.1. The Monte Carlo method

In this study, we consider the Monte Carlo method as a method of statistical modeling of the complex photochemical system that allows random perturbations of its parameters (Vorobeva et al., 2018).

The general principle of the Monte Carlo method can be described in three successive steps:

1. Generating of pseudo-random numbers with the necessary characteristics for simulation of randomly changing of the model parameters.
2. Using the perturbed parameters in the model.
3. Statistical processing of the simulation results (calculation of the mean, standard deviation and coefficient of variation as an indicator of the model variation).

As stated previously, the YM2011 model contains a large number of parameters that can vary randomly and independently. The perturbation of each model parameter influences the simulation result and is described by the distribution function and the amplitude value of the error (typical values of the relative errors of the model parameters are presented in Table 2).

For a simulation of random changing of each model parameter z, we used a factor

$$\Lambda_z = 1 + \xi_z \cdot a_{rnd}, \tag{3}$$

where a_{rnd} is a pseudo-random number from interval $[-1; 1]$.

This approach allows generating a pseudo-random number Λ_z within $[1 - \xi_z;\ 1 + \xi_z]$. The product $z{\cdot}\Lambda_z$ takes values within a range of $[z - \Delta z;\ z + \Delta z]$.

Most experimenters assume that experimentally determined errors of the parameters have a uniform distribution function. However, a number of studies also refer to the normal error distribution function. For this reason, in this study, calculations were performed for both uniform and normal error distribution functions.

The distribution of the error directly depends on the distribution function of the pseudo-random number a_{rnd} from (3). We used a standard generator (Forsythe et al., 1977) for the creation of pseudo-random numbers with a uniform distribution function. In the case of generating pseudo-random numbers with a normal distribution function, several comments should be made.

1. The pseudo-random number generator is based on the generation of numbers with a uniform distribution function (Forsythe et al., 1977).
2. The mean is assumed to be zero.
3. The standard deviation is assumed to be 0.5 in order to the most of the generated numbers fall within $[-1; 1]$. In this case, 95% of the generated numbers fall within a range of $[-1; 1]$, equivalent to $[-2\sigma; 2\sigma]$.

The Monte Carlo method does not have a high convergence rate, which implies a large number of runs. We

Table 1
The wavelengths of the centers of the Atmospheric and IR Atmospheric O_2 bands, Einstein coefficients for the corresponding transitions, A_E, and radiative lifetimes of the states $O_2(b^1\Sigma_g^+,\ v' \le 2)$ and $O_2(a^1\Delta_g,\ v' \le 5)$, τ.

Transitions	$O_2(X^3\Sigma_g^-,\ v''=0)$		$O_2(X^3\Sigma_g^-,\ v''=1)$		$O_2(X^3\Sigma_g^-,\ v''=2)$		τ, s
	λ, nm	A_E, s^{-1}	λ, nm	A_E, s^{-1}	λ, nm	A_E, s^{-1}	
O_2 Atm band (v', v'')							
$O_2(b^1\Sigma_g^+,\ v'=0)$	762.1	8.50E-02	864.7	4.19E-03	996.8	1.04E-04	1.10E+01
$O_2(b^1\Sigma_g^+,\ v'=1)$	688.4	8.28E-03	771.0	6.98E-02	874.4	8.04E-03	1.14E+01
$O_2(b^1\Sigma_g^+,\ v'=2)$	628.8	4.36E-04	697.0	1.58E-02	780.4	5.54E-02	1.18E+01
O_2 IR Atm band (v', v'')							
$O_2(a^1\Delta_g,\ v'=0)$	1268.6	2.26E-04	1580.7	1.53E-06	2086.1	6.50E-09	4.40E+03
$O_2(a^1\Delta_g,\ v'=1)$	1067.7	5.00E-06	1280.4	2.13E-04	1593.1	3.23E-06	4.52E+03
$O_2(a^1\Delta_g,\ v'=2)$	924.0	4.03E-08	1079.1	1.05E-05	1293.0	2.00E-04	4.64E+03
$O_2(a^1\Delta_g,\ v'=3)$	816.1	5.16E-13	934.9	1.47E-07	1091.2	1.64E-05	4.77E+03
$O_2(a^1\Delta_g,\ v'=4)$	732.3	4.19E-11	826.4	3.92E-11	946.3	3.55E-07	4.92E+03
$O_2(a^1\Delta_g,\ v'=5)$	665.2	5.87E-12	742.0	1.80E-10	837.3	5.10E-10	5.07E+03

Table 2
The amplitude values of the relative errors of the YM2011 model parameters used in this study.

YM2011 model parameter, z	The amplitude value of the relative error, ξ_z	References
Parameters of the background atmosphere (pressure, kinetic temperature and gas density)	1%	Picone et al. (2002), Rezac et al. (2015)
Rates of the photo excitation processes (J_{SRC}, J_{Lya}, J_{HHB}, g_α, g_β, g_γ and g_{IRa})	1%	Calculation using parameters of the background atmosphere (Yankovsky et al., 2007) and spectral composition of solar radiation (SORCE, 2003)
Einstein coefficients for transitions in O_2 Atmospheric bands	3%–10%	Krupenie (1972), Gamache and Goldman (2001), Yu et al. (2014), Simeckova et al. (2006)
Rate coefficients and quantum yields of reaction products	Values of errors are from a percent to several tens of percent	Atkinson et al. (2004), Burkholder et al. (2015), Yankovsky et al. (2016), Yankovsky and Manuilova (2018)
Measured concentrations of O_3, $O(^3P)$ and CO_2 (for forward problems, Section 4)	10–20%	Smith et al. (2013), Hedin et al. (2009), Rezac et al. (2015)

carried out tests for the number of runs from 500 to 10,000. In this paper, the results of calculations are given for the number of runs equal to 5000, since a further increase in the number of runs did not significantly change the results of the numerical experiment in all the considered cases.

3.2. The sensitivity analysis

If the target component x depends on n parameters z_i, the sensitivity analysis can be used to estimate the relative uncertainty of x (Yankovsky et al., 2016). The sensitivity coefficient of the target component to the variation of parameter z, $S(x; z)$, is:

$$S(x;z) = \frac{z}{x}\frac{\partial x}{\partial z}. \quad (4)$$

The relative uncertainty of the target component x is related to the sensitivity coefficients, as well as to the relative errors of all model parameters, $\xi_{z,i}$:

$$\frac{\Delta x}{x} = \sqrt{\sum_{i=1}^{n} (S(x;z_i))^2 (\xi_{z,i})^2}. \quad (5)$$

We applied this approach to solving both the forward and inverse problems. The sensitivity analysis to all model parameters was carried out for determining $[O(^3P)]$ and $[O_3]$ (Yankovsky et al., 2016), as well as for determining $[CO_2]$ (Yankovsky and Manuilova, 2018). z_i are the parameters of the YM2011 model, such as concentrations of the main background atmosphere components, the kinetic temperature, the rates of photoexcitation processes, the quantum yields of reaction products, the rate coefficients of quenching reactions of the component x in the radiative and collisional processes, and also volume emission rates.

4. Estimation of the uncertainty of the forward problem solution

In this study we investigate the forward problems to calculate the altitude profiles of $[O(^1D)]$, $[O_2(b^1\Sigma_g^+, v \le 2)]$ and $[O_2(a^1\Delta_g, v = 0)]$.

The altitude profile of the excited component concentration was calculated from balance equation which is a particular case of the kinetic equation in the case of quasi-stationary conditions and it takes into account all the channels of level excitation and quenching which are typical of the MLT region. Kinetic equations for excited levels considered were taken from (Yankovsky et al., 2016). The general form of a balance equation is:

$$[x] = \frac{P(x)}{Q(x)}, \quad (6)$$

where $[x]$ is the concentration of excited molecules of $O_2(b^1\Sigma_g^+, v \le 2)$, $O_2(a^1\Delta_g, v = 0)$ or an atom $O(^1D)$ (in cm^{-3}); $P(x)$ is the production rate of the x (in $cm^{-3}s^{-1}$); $Q(x)$ is a quenching factor of the x in the radiative and collisional processes (in s^{-1}).

Quenching factor $Q(x)$ of the component x is:

$$Q(x) = (\tau)^{-1} + [N_2]\cdot k(x;N_2) + [O_2]\cdot k(x;O_2) + [O_3]\cdot k(x;O_3) + [O(^3P)]\cdot k(x;O(^3P)) + [CO_2]\cdot k(x;CO_2). \quad (7)$$

It takes into account both radiative deexcitation and quenching at collisions with the major components of the atmosphere (O_2, N_2, $O(^3P)$, O_3, CO_2). The contribution of O_2, N_2, $O(^3P)$, O_3, CO_2 to the quenching of proxies $O(^1D)$, $O_2(b^1\Sigma_g^+, v = 0–2)$ and $O_2(a^1\Delta_g, v = 0)$ was described in detail in Yankovsky and Manuilova (2018). Radiative lifetimes, τ, are presented in Table 1. Total database of rate coefficients and quantum yields for collisional reactions involving $O(^1D)$, $O_2(b^1\Sigma_g^+, v \le 2)$, $O_2(a^1\Delta_g, v = 0–5)$ is presented in the Supplementary Material.

To estimate the uncertainty of the forward problem solution, it is necessary to take into account a random and independent change of each parameter of the balance equation. We performed the uncertainty estimation by the two ways outlined above: sensitivity analysis (Section 3.2) and the Monte Carlo method (Section 3.1).

The calculations were carried out for various events of the TIMED-SABER experiment depending on the seasons

of the year, latitude, solar zenith angle. For each event, we calculated the rates of photoprocesses in the Hartley and Huggins bands, the Schumann-Runge continuum, H Lyman-α line, and the rates of the resonant excitation processes of $O_2(b^1\Sigma_g^+, v = 2, 1, 0)$ and $O_2(a^1\Delta_g, v = 0)$ (g_α, g_β, g_γ and g_{IRa}, respectively) were calculated from the SORCE solar spectrum (SORCE, 2003) and cross-section database (Atkinson et al., 2004) with reference to fixed wavelengths by the technique described in Yankovsky et al. (2007). However, in this study, in the Figures we present calculations for the typical event: SABER L2, 2010, day 172, latitude 43.0, SZA = 70.5, F10.7 = 74. We do not use the F10.7 solar index to calculate the rates of photo processes. Information about F10.7 is included in the standard description of SABER events.

4.1. Estimation of the uncertainty of the forward problem solution by the example of $[O(^1D)]$ altitude profile calculation

A detailed description of the application of the sensitivity analysis to estimating the uncertainty of the target function retrieval is presented in Yankovsky et al. (2016). In this regard, in the following we describe only the application of the Monte Carlo method.

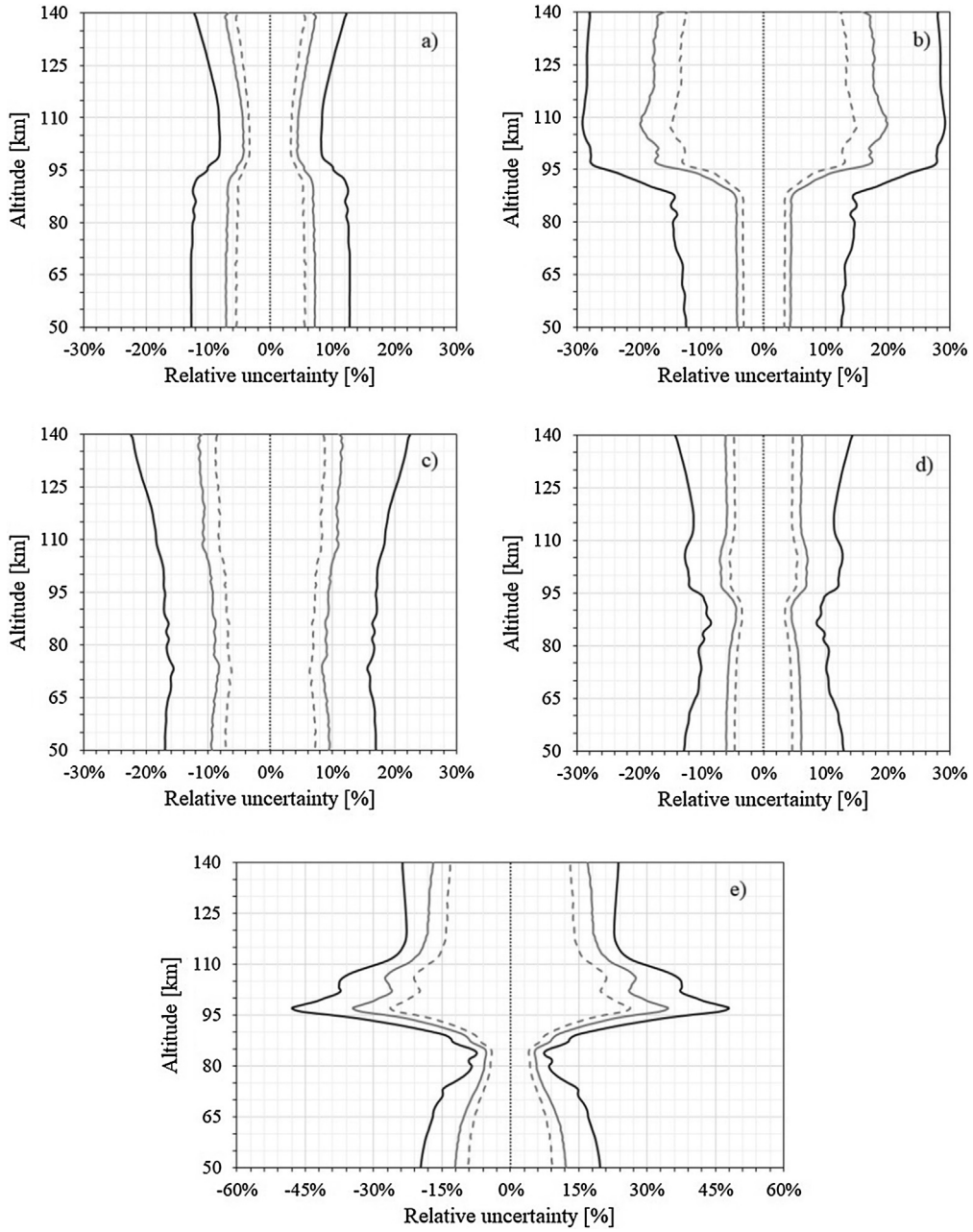

Fig. 2. Altitude dependence of the calculated relative uncertainty of: (a) $[O(^1D)]$, (b) $[O_2(b^1\Sigma_g^+, v = 2)]$, (c) $[O_2(b^1\Sigma_g^+, v = 1)]$, (d) $[O_2(b^1\Sigma_g^+, v = 0)]$, (e) $[O_2(a^1\Delta_g, v = 0)]$. Legend: reference (black dotted line); results of the Monte Carlo simulation with the uniform (grey solid line) and the normal (grey dashed line) error distribution functions; results of the sensitivity analysis (black solid line).

In this section we demonstrate the practical use of a random factor (3) in the Monte Carlo method by using the balance equation for the excited oxygen atom as an example.

The balance equation for $[O(^1D)]$ is

$$[O(^1D)] = \frac{[O_2]\cdot\left(J_{SRC} + J_{Ly\alpha}\cdot F(Ly\alpha)\right) + [O_3]\cdot J_{HHB}\cdot F(HHB)}{Q(O(^1D))}. \quad (8)$$

After the application of a random factor (3) to each parameter, the balance Eq. (6) transforms to:

$$[O(^1D)] = \frac{[O_2]\cdot\Lambda_{O_2}\cdot\left(J_{SRC}\cdot\Lambda_{J_{SRC}} + J_{Ly\alpha}\cdot\Lambda_{J_{Ly\alpha}}\cdot F(Ly\alpha)\cdot\Lambda_{F(Ly\alpha)}\right) + [O_3]\cdot\Lambda_{O_3}\cdot J_{HHB}\cdot\Lambda_{J_{HHB}}\cdot F(HHB)\cdot\Lambda_{F(HHB)}}{Q_\Lambda(O(^1D))}, \quad (8')$$

where "perturbed" quenching factor $Q_\Lambda(O(^1D))$ has a form different from the "unperturbed" quenching factor $Q(O(^1D))$ (7):

$$Q_\Lambda(O(^1D)) = \tau^{-1}_{O(^1D)} + [O_2]\cdot\Lambda_{O_2}\cdot k(O(^1D);O_2)\cdot\Lambda_{k(O(^1D);O_2)} + [N_2]\cdot\Lambda_{N_2}\cdot k(O(^1D);N_2)\cdot\Lambda_{k(O(^1D);N_2)} + [CO_2]\cdot\Lambda_{CO_2}\cdot k(O(^1D);CO_2)\cdot\Lambda_{k(O(^1D);CO_2)} + [O_3]\cdot\Lambda_{O_3}\cdot k(O(^1D);O_3)\cdot\Lambda_{k(O(^1D);O_3)} + [O(^3P)]\cdot\Lambda_{O(^3P)}\cdot k(O(^1D);O(^3P))\cdot\Lambda_{k(O(^1D);O(^3P))}. \quad (7')$$

A pseudo-random number a_{rnd} with the required distribution function is generated at each step for each parameter z. In other words, pseudo-random numbers at (7′) and (8′) do not correlate with each other.

Fig. 2a demonstrates the simulation results by (8′). The Monte Carlo method gives an estimation of the relative uncertainty of the $[O(^1D)]$ altitude profile of about 4–7% and 3–6% for the uniform and normal error distribution function, respectively. The sensitivity analysis, which takes into account the amplitude errors of the parameters, gives an estimation of the $[O(^1D)]$ altitude profile uncertainty within 8–13%. The proxy $O(^1D)$ has relatively small uncertainty values since all parameters of the Eq. (8) are known quite accurately (Yankovsky et al., 2016).

4.2. The uncertainties of calculations of the $[O_2(b^1\Sigma_g^+, v = 0–2)]$ and $[O_2(a^1\Delta_g, v = 0)]$ altitude profiles

In this section we present full balance equations for excited oxygen molecules $O_2(b^1\Sigma_g^+, v = 0–2)$ and $O_2(a^1\Delta_g, v = 0)$ based on YM2011 model.

$$[O_2(b, v = 2)] = [O_2]\cdot\frac{g_\gamma}{Q(O_2(b, v = 2))}, \quad (9)$$

$$[O_2(b, v = 1)] = \frac{[O_2]\cdot\left(g_\beta + [O(^1D)]\cdot k(O(^1D);O_2)\cdot\psi_1\right) + [O_2(b, v = 2)]\cdot[O(^3P)]\cdot k(O_2(b, v = 2);O(^3P))\cdot\psi_{b,2\to b,1}}{Q(O_2(b, v = 1))}, \quad (10)$$

$$[O_2(b, v = 0)] = \frac{1}{Q(O_2(b,v=0))}\{[O_2]\cdot(g_\alpha + [O(^1D)]\cdot k(O(^1D);O_2)\cdot\psi_0 + [O_2(b, v = 1)]\cdot k(O_2(b, v = 1);O_2)) + [O_2(b, v = 2)]\cdot\left([O_2]\cdot k(O_2(b, v = 2);O_2) + [O(^3P)]\cdot k(O_2(b, v = 2);O(^3P))\cdot\psi_{b,2\to b,0}\right)\}, \quad (11)$$

$$[O_2(a, v = 0)] = \frac{[O_3]\cdot J_{HHB}\cdot F(HHB\to a, 0) + [O_2]\cdot\left(g_{IRa} + \sum_{v=1}^{5}[O_2(a, v)]\cdot k(O_2(a, v);O_2)\right)}{Q(O_2(a, v = 0))} + \frac{[O_2(b, v = 0)]}{Q(O_2(a, v = 0))}\cdot\left\{[O_2]\cdot k(O_2(b, v = 0);O_2)\cdot\psi^{O_2}_{b,0\to a,0} + [O(^3P)]\cdot k(O_2(b, v = 0);O(^3P))\cdot\psi^{O(^3P)}_{b,0\to a,0} + [O_3]\cdot k(O_2(b, v = 0);O_3)\cdot\psi^{O_3}_{b,0\to a,0} + [CO_2]\cdot k(O_2(b, v = 0);CO_2)\cdot\psi^{CO_2}_{b,0\to a,0}\right\}. \quad (12)$$

We do not demonstrate "perturbed" counterparts of Eqs. (9)–(12) (taking into account random variations of the parameters) because of their complexity. We carried out a simulation similar to the one described in Section 4.1 for each of the molecular levels, $O_2(b^1\Sigma_g^+, v = 0–2)$ and $O_2(a^1\Delta_g, v = 0)$. Fig. 2 (b-e) presents the simulation results.

Fig. 2 shows that the uncertainty values of the forward problem solution, obtained by means of a sensitivity analysis, exceed the values obtained by using the Monte Carlo method in all considered cases. We suggest the reason is that the sensitivity analysis is based on the use of the amplitude values of the errors, while the Monte Carlo method allows to vary each parameter z_i within its error, taking into account the distribution function of the error.

In general, the results of statistical modeling are consistent with the results of the sensitivity analysis presented in Yankovsky et al. (2016). The maximum uncertainty of the

solution is observed at the calculation of $[O_2(a^1\Delta_g, v=0)]$ altitude profile. We suggest that this is directly related to the large number of parameters taken into account (more than 25 parameters), as well as large errors of some rate coefficients.

The sensitivity analysis (Yankovsky et al., 2016) showed that for each proxy there is a group of the most significant parameters, which we call the key parameters. It should be noted the influence of the key parameter errors on the uncertainty of the forward problem solution. This is clearly expressed for the two forward problems: calculation of $[O_2(b^1\Sigma_g^+, v=2)]$ altitude profile (Fig. 2b) and calculation of $[O_2(a^1\Delta_g, v=0)]$ altitude profile (Fig. 2e). In both cases, the uncertainty greatly increases above 85 km. The reason of this effect is the high $[O(^3P)]$ above the mesopause region, as well as the fact that the rate coefficients $k(O_2(b, v=2); O(^3P))$ and $k(O_2(a, v=0); O(^3P))$ are known with relatively large errors: $\xi_{k(O2(b,\ v=2);\ O(3P))} = 0.3$ and $\xi_{k(O2(a,\ v=0);\ O(3P))} = 2.0$, respectively. At the same time, the quenching rate coefficients in collisions with O_2 and N_2 have error values an order of magnitude smaller. For the other proxies considered, the rate coefficients of quenching reactions in collisions with $O(^3P)$ and molecular components O_2, N_2, CO_2, O_3 have comparable error values (Table A1 in Yankovsky et al., 2016); therefore, the uncertainty of the forward problem solution varies slightly with altitude.

One more result should be noted, namely, decrease of the uncertainty for $O_2(a^1\Delta_g, v=0)$ above 95 km. The contribution of ozone to the production of $O_2(a^1\Delta_g, v=0)$ rapidly decreases above 95 km and is replaced by the contribution of energy transfer from $O(^1D)$ that is produced as a result of O_2 photodissociation in Schumann-Runge continuum. Energy of excited atom $O(^1D)$ is spent on the excitation of $O_2(b^1\Sigma_g^+, v=1)$, and then on the excitation of $O_2(b^1\Sigma_g^+, v=0)$. Rate coefficients of the reactions describing this energy transfer are known with good accuracy [Supplemental material], and it leads to a decrease of the relative uncertainty of $O_2(a^1\Delta_g, v=0)$ above 95 km.

5. Methods for retrieving the $[O_3]$, $[O(^3P)]$ and $[CO_2]$ altitude profiles. Estimations of uncertainties of the retrieved concentrations

The inverse problem is to retrieve the concentrations of hard-to-measure small components of the atmosphere based on the observed volume emission rates of the excited oxygen. A typical example of the inverse problem is the retrieval of the ozone concentration from observations of the volume emission rate of the O_2 IR Atmospheric band at a wavelength of 1.27 μm.

When using the Monte Carlo method, it is necessary to have an analytical expression for determining a concentration of the target component. In this section, all analytical expressions are derived from the balance Eqs. (8)–(12) based on the sensitivity analysis conducted in Yankovsky et al. (2016). In these balance equations, we neglect the processes whose influence on the result of the retrieval of the target component does not exceed 0.1% (in some cases 1%) in the MLT region.

Further, we present the discarded processes in each specific case of the retrieval. Note some common simplifications:

(i) Yankovsky and Manuilova (2018) showed that quenching at collisions with CO_2 is essential for the only one proxy, $O_2(b^1\Sigma_g^+, v=0)$. Thus, for other proxies, $O(^1D)$, $O_2(b^1\Sigma_g^+, v=2)$, $O_2(b^1\Sigma_g^+, v=1)$ and $O_2(a^1\Delta_g, v=0)$, we did not take into account this quenching process.

(ii) In the balance Eqs. (10)–(12), $[O_2(b^1\Sigma_g^+, v=2)]$ can be discarded since the sensitivity coefficients to this parameter are less than 0.01% (Yankovsky et al., 2016).

Practically, for using any of the proposed methods for solving inverse problems in order to retrieve the target components, information is needed on the errors of both the "internal" parameters of the model (Table 2) and the measured values (proxy concentration). In each particular experiment, these values may depend on the capabilities of the experimental equipment. In satellite experiments (Shmakov and Ustinov, 1994; Picone et al., 2002), the accuracy of measurements of the intensity of the O_2 Atmospheric band at 1.27 μm reached about 1%. In our numerical experiments, we take the error of the measured values of 1%.

5.1. Retrieval of the altitude profile of O_3 concentration

In the MLT below ~98 km the ozone concentration can be retrieved by using emissions of the next proxies: $O(^1D)$, $O_2(b^1\Sigma_g^+, v=1)$, $O_2(b^1\Sigma_g^+, v=0)$ and $O_2(a^1\Delta_g, v=0)$ (Yankovsky et al., 2016). Retrieval of the $[O_3]$ from the proxy $O_2(b^1\Sigma_g^+, v=2)$ is impossible as sensitivity coefficient is too small, $S(O_3; O_2(b, v=2)) < 0.1\%$. This section successively presents analytical expressions for retrieving the ozone concentration from the listed proxies.

Random changing of each model parameter was carried out similar to the procedure described in Section 4.1. In each specific case, we used $[O_3]$ altitude profile predetermined via presented analytical expression as a reference. Then we varied each of the model parameters in the corresponding experimentally well-founded limits of the error using random factors of the form (3). Fig. 3(a-d) demonstrates the comparison of the results obtained by the sensitivity analysis with the results obtained by the Monte Carlo method.

5.1.1. Retrieval of $[O_3]$ from $[O(^1D)]$

In the balance Eq. (8) for the altitude range of 50–100 km, the following processes were discarded:

- Radiative deexcitation $O(^1D) \rightarrow O(^3P) + h\nu$ (630.0 and 636.4 nm) since $S(O(^1D); \tau_{O(1D)}) < 0.07\%$;

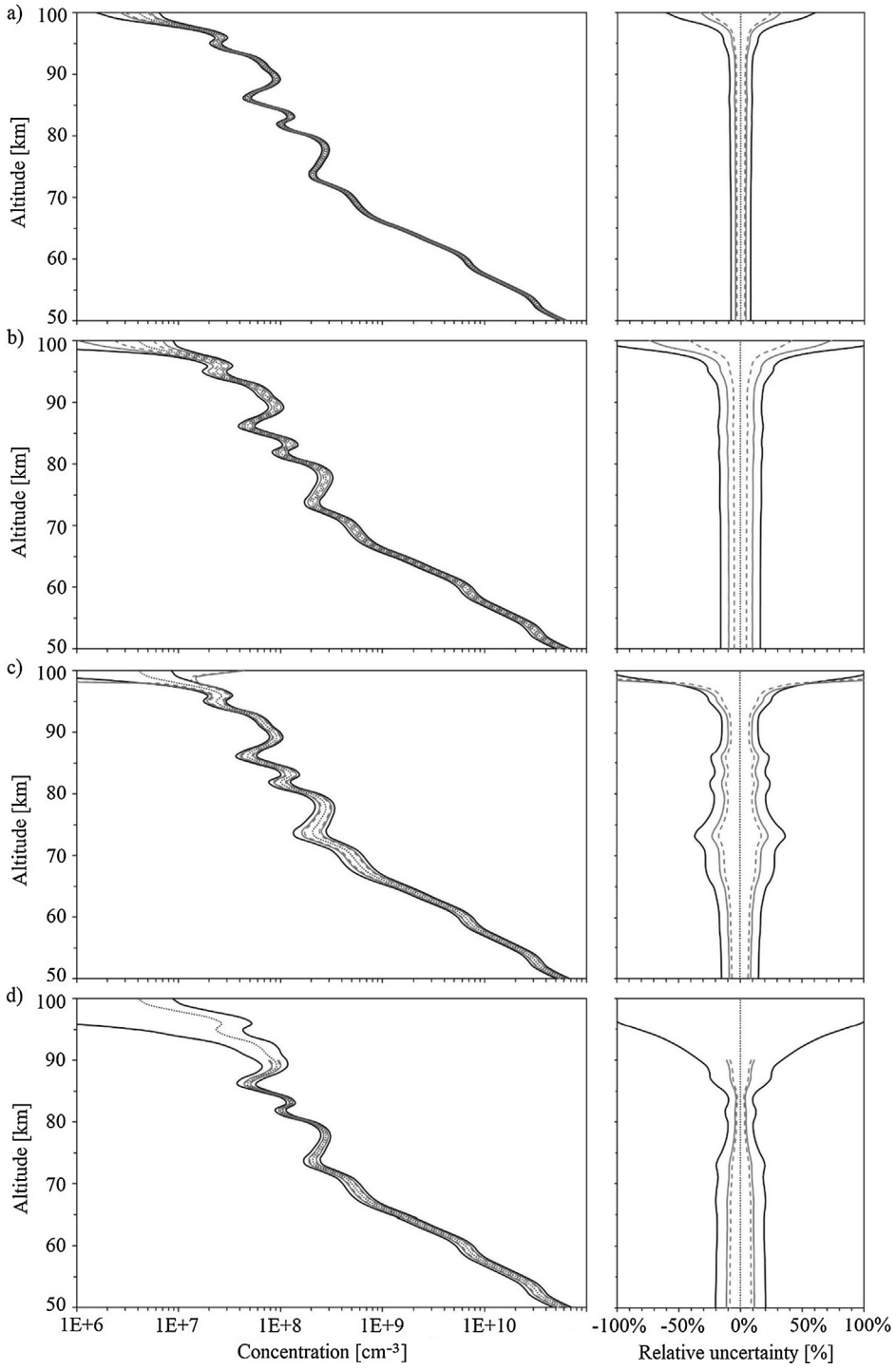

Fig. 3. Altitude dependence of the calculated relative uncertainty of the $[O_3]$ altitude profile retrieved from the next proxies: (a) $O(^1D)$, (b) $O_2(b^1\Sigma_g^+, v = 1)$, (c) $O_2(b^1\Sigma_g^+, v = 0)$, (d) $O_2(a^1\Delta_g, v = 0)$. Left panel presents absolute uncertainty, right panel presents relative uncertainty. Legend: reference (black dotted line); results of the Monte Carlo simulation with the uniform (grey solid line) and the normal (grey dashed line) error distribution functions; results of the sensitivity analysis (black solid line).

- Collisional quenching in the reaction $O(^1D) + O_3 \rightarrow O_2 + 2O(^3P)$ since $S(O(^1D); O_3) < 0.003\%$.

Using these simplifications, we derived the analytical expression for retrieving the ozone concentration from $[O(^1D)]$ in the MLT:

$$[O_3] = \frac{1}{J_{HHB} \cdot F(HHB)} \cdot \{[O(^1D)] \cdot ([O_2] \cdot k(O(^1D); O_2) + [N_2] \cdot k(O(^1D); N_2) + [O] \cdot k(O(^1D); O(^3P))) - [O_2] \cdot (J_{SRC} + J_{Ly\alpha} \cdot F(Ly\alpha))\}, \quad (13)$$

where measured parameter is [O(^{1}D)] which is determined from the volume emission rate from this excited level of oxygen atom in the line 630.0 nm.

Fig. 3a displays the uncertainty of [O_3] retrieved from [O(^{1}D)] depending on altitude. Similar to Section 4, the sensitivity analysis shows an overestimated value of the uncertainty for the whole altitude interval. The uncertainty obtained by the Monte Carlo method does not exceed 6% for the altitude range of 50–90 km. Only above 90 km, the uncertainty gradually increases to 34% at 100 km. The reason is that ozone concentration decreases above 90 km, therefore ozone ceases to be a source of O(^{1}D) in range 90–100 km and gives way to photolysis of molecular oxygen. Thus, the relative uncertainty of retrieval increases.

5.1.2. Retrieval of [O_3] from [$O_2(b^1\Sigma_g^+,\ v=1)$]

Based on sensitivity analysis, the reactions $O_2(b^1\Sigma_g^+,\ v=1)+O_3\rightarrow$ *products* and $O_2(b^1\Sigma_g^+,\ v=1)+N_2\rightarrow$ *products* can be neglected in the balance Eq. (10) in addition to the common simplifications (see above).

Using these simplifications, (Yankovsky et al., 2016) presented the analytical expression for retrieving the ozone concentration from [$O_2(b^1\Sigma_g^+,\ v=1)$] in the altitude range of 50–98 km:

$$[O_3]=\frac{1}{J_{HHB}\cdot F(HHB)}\cdot\left\{\frac{([O_2(b,v=1)]\cdot Q(O_2(b,v=1))-[O_2]\cdot g_\beta)\cdot Q(O(^1D))}{[O_2]\cdot k(O(^1D);O_2)\cdot\psi_1}-[O_2]\cdot\left(J_{SRC}+J_{Ly\alpha}\cdot F(Ly\alpha)\right)\right\},\qquad(14)$$

where [$O_2(b^1\Sigma_g^+,\ v=1)$] is determined by the volume emission rate from this level using the Einstein coefficients for the corresponding O_2 Atmospheric bands (Table 1).

5.1.3. Retrieval of [O_3] from [$O_2(b^1\Sigma_g^+,\ v=0)$]

In Martyshenko and Yankovsky (2017), the method of retrieving the [O_3] from [$O_2(b^1\Sigma_g^+,\ v=0)$] was investigated in detail and it was proved that the following reactions can be neglected in the balance Eq. (11): $O_2(b^1\Sigma_g^+,\ v=0)+O_3\rightarrow$ *products* and $O_2(b^1\Sigma_g^+,\ v=0)+O_2\rightarrow$ *products*.

Using these simplifications, we derived the analytical expression for retrieving the ozone concentration from [$O_2(b^1\Sigma_g^+,\ v=0)$] in the altitude range of 50–85 km:

$$[O_3]=\frac{1}{J_{HHB}\cdot F(HHB)}\cdot\left\{\left(1+\frac{[O(^3P)]\cdot k(O(^1D);O(^3P))+[N_2]\cdot k(O(^1D);N_2)}{[O_2]\cdot k(O(^1D);O_2)}\right)\times([O_2(b,v=0)]\cdot Q(O_2(b,v=0))-[O_2]\cdot(g_\alpha+g_\beta))-[O_2]\cdot\left(J_{SRC}+J_{Ly\alpha}\cdot F(Ly\alpha)\right)\right\}.\qquad(15)$$

Fig. 3c shows the uncertainty of [O_3] retrieved from [$O_2(b^1\Sigma_g^+,\ v=0)$] depending on altitude. The uncertainty obtained by the Monte Carlo method takes values from 7% to 21% in the altitude range of 50–85 km. As in the previous paragraphs of this section, the uncertainty begins to grow rapidly above 85 km. The uncertainty noticeably varies with altitude, thus we can conclude that $O_2(b^1\Sigma_g^+,\ v=0)$ is not the best proxy.

5.1.4. Retrieval of [O_3] from [$O_2(a^1\Delta_g,\ v=0)$]

In Martyshenko and Yankovsky (2017), the method for retrieving the [O_3] from [$O_2(a^1\Delta_g,\ v=0)$] was investigated in detail. In Martyshenko and Yankovsky (2017) some simplifications were made. In particular, collisional reactions with atomic oxygen were not considered, therefore, the proposed method for retrieving the [O_3] can be utilized only below 90 km. The next analytical expression for [O_3] in the altitude range of 50–90 km was obtained:

$$[O_3]=\frac{[O_2(a,v=0)]\cdot Q(O_2(a,v=0))-[O_2]\cdot\left(g_{IRa}+(g_\alpha+g_\beta)\cdot\zeta\cdot\frac{[N_2]\cdot k(O_2(b,v=0);N_2)}{Q(O_2(b,v=0))}\right)}{J_{HHB}\cdot F(HHB)\cdot\left(\tilde{F}+\zeta\cdot\frac{[N_2]\cdot k(O_2(b,v=0);N_2)}{Q(O_2(b,v=0))}\cdot\frac{[O_2]\cdot k(O(^1D);O_2)}{Q(O(^1D))}\right)},\qquad(16)$$

Fig. 3b displays the uncertainty of retrieval of the [O_3] altitude profile from [$O_2(b^1\Sigma_g^+,\ v=1)$] altitude profile. The uncertainty obtained by the Monte Carlo method takes values from 6% to 13% for the altitude range of 50–97 km. The uncertainty increases rapidly above 97 km.

where ζ is a quantum yield of $O_2(a^1\Delta_g,\ v=2)$ formation in the reaction $O_2(b^1\Sigma_g^+,\ v=0)+N_2\rightarrow$ *products*, equal to 0.5; $\tilde{F}$ is a total (accumulated) quantum yield of $O_2(a^1\Delta_g,\ v=0)$ molecules by ozone photolysis in the Hartley band, equal to 0.95 ± 0.05.

Note that (Wu et al., 2018) used a simplified version of the formula (16) to interpret the volume emission rate of $O_2(a^1\Delta_g,\ v=0)$ band at 1.27 μm under observations via DASH-interferometer (the Doppler Asymmetric Spatial Heterodyne) designed for limb-viewing satellites. The parameters g_{IRa} and g_β were discarded; it was assumed that $\widetilde{F}=1$.

It is hard to agree with one more simplification in work (Wu et al., 2018). The authors believed that the molecules $O_2(b^1\Sigma_g^+,\ v=0)$ are formed in reaction $O(^1D)+O_2\rightarrow O(^3P)+O_2(b^1\Sigma_g^+,\ v)$ with an effective quantum yield of 0.54–1.0. This point of view really existed in the 90 s, but was rejected because of the absence of any details of such a kinetic mechanism. The fact is that in 2014 for reaction $O(^1D)+O_2\rightarrow O(^3P)+O_2(b^1\Sigma_g^+,\ v\le 1)$, the quantum yields of the formation of the molecules $O_2(b^1\Sigma_g^+,\ v=1)$ and $O_2(b^1\Sigma_g^+,\ v=0)$ were measured, $\psi_1=(0.80\pm0.10)$, and $\psi_0=(0.20\pm0.10)$, respectively (Pejakovic et al., 2014). Using the YM2011 model, we examined in detail the relaxation mechanism of the $O_2(b^1\Sigma_g^+,\ v=1)$ to the level of $O_2(b^1\Sigma_g^+,\ v=0)$ and obtained formula (16) (Yankovsky et al., 2016; Martyshenko and Yankovsky, 2017).

Fig. 3d demonstrates the uncertainty of $[O_3]$ retrieved from $[O_2(a^1\Delta_g,\ v=0)]$ depending on altitude by using the formula (16). As seen, the uncertainty obtained by the Monte Carlo method does not exceed 12% in the altitude range of 50–90 km. We have a numerical solution of the inverse problem in the entire altitude range, however, we were unable to construct an analytical expression for determining $[O_3]$ from this proxy above 90 km. On the other hand, the sensitivity analysis performed with no simplifications based on balance Eq. (12) shows a very fast increase of the uncertainty above 90 km (up to 100% and more) due to the large error of the rate coefficient $k(O_2(a,\ v=0);\ O(^3P))$. Thus, the proxy $[O_2(a^1\Delta_g,\ v=0)]$ can be used to retrieve $[O_3]$ only below 88–89 km.

5.2. Retrieval of the altitude profile of $O(^3P)$ concentration

Atomic oxygen concentration can be retrieved above 90 km by using emissions of the next proxies: $O(^1D)$, $O_2(b^1\Sigma_g^+,\ v=2)$, $O_2(b^1\Sigma_g^+,\ v=1)$ and $O_2(b^1\Sigma_g^+,\ v=0)$ (Yankovsky et al., 2016). The lower limit of altitude is explained by the fact that the sensitivity coefficients of these proxies to $O(^3P)$ are close to zero below 90 km. This section successively presents analytical expressions for retrieving the atomic oxygen concentration from the listed proxies. Fig. 4(a–d) demonstrates the comparison of the results obtained by the sensitivity analysis with the results obtained by the Monte Carlo method.

5.2.1. Retrieval of $[O(^3P)]$ from $[O(^1D)]$

It is possible to neglect the radiative deexcitation and the reaction $O(^1D)+O_3\rightarrow products$ in the balance Eq. (8) based on the sensitivity analysis (Yankovsky et al., 2016; Yankovsky and Manuilova, 2018).

Using these simplifications, in this study we derived the analytical expression for retrieving atomic oxygen concentration from $[O(^1D)]$ in the altitude range of 90–140 km:

$$\left[O(^3P)\right]=\frac{[O_2]\cdot\left(J_{SRC}+J_{Ly\alpha}\cdot F(Ly\alpha)\right)+[O_3]\cdot J_{HHB}\cdot F(HHB)}{\left[O(^1D)\right]\cdot\ k\left(O(^1D);O(^3P)\right)}-\frac{[O_2]\cdot k\left(O(^1D);O_2\right)+[N_2]\cdot\ k\left(O(^1D);N_2\right)}{k\left(O(^1D);O(^3P)\right)}. \tag{17}$$

As can be seen from Fig. 4a, the uncertainty of retrieval of $[O(^3P)]$ from this proxy is very large (>100%) below 100 km. The uncertainty gradually decreases with increasing altitude, but even in the region of 115 km it exceeds 20%. This suggests that $O(^1D)$ has a low sensitivity to the concentration of atomic oxygen in the lower thermosphere. However, sensitivity to $[O(^3P)]$ increases above 150 km (Witasse et al., 1999). We suppose that the question of using the proxy $O(^1D)$ in the intermediate interval of 115–150 km requires additional research.

5.2.2. Retrieval of $[O(^3P)]$ from $[O_2(b^1\Sigma_g^+,\ v=2)]$

The reaction $O_2(b^1\Sigma_g^+,\ v=2)+O_3\rightarrow products$ can be discarded in the balance Eq. (9) since ozone concentration decreases rapidly above 90 km and the sensitivity coefficient $S(O_2(b,\ v=2);\ O_3)<0.1\%$. Thus, in this study we derived the analytical expression for retrieving $[O(^3P)]$ in the altitude range 90–140 km:

$$\left[O(^3P)\right]=\frac{\frac{[O_2]\cdot g_\gamma}{[O_2(b,v=2)]}-\left(\tau^{-1}_{O_2(b,v=2)}+[O_2]\cdot k(O_2(b,v=2);O_2)+[N_2]\cdot k(O_2(b,v=2);N_2)\right)}{k(O_2(b,v=2);O(^3P))}, \tag{18}$$

where $[O_2(b^1\Sigma_g^+,\ v=2)]$ is determined by the volume emission rate from this level using the Einstein coefficients for the corresponding O_2 Atmospheric bands (Table 1).

Fig. 4b shows the results of statistical modeling using formula (18). The uncertainty of $[O(^3P)]$ retrieval from $[O_2(b^1\Sigma_g^+,\ v=2)]$ obtained by the Monte Carlo method depends slightly on the altitude in the recommended altitude range and takes values of 17–20%. The obtained results are consistent with the conclusions made on the basis of the sensitivity analysis (Yankovsky et al., 2016).

5.2.3. Retrieval of [$O(^3P)$] from [$O_2(b^1\Sigma_g^+, v = 1)$]

Yankovsky et al. (2016) described the method for retrieving the [$O(^3P)$] altitude profile from [$O_2(b^1\Sigma_g^+, v = 1)$] in detail and demonstrated that it is necessary to solve the quadratic equation (the positive value of the equation root is chosen). The analytical expression for retrieving atomic oxygen concentration from proxy $O_2(b^1\Sigma_g^+, v = 1)$ in the altitude range of 90–140 km was presented:

$$[O(^3P)] = \frac{B - A}{2} + \sqrt{\frac{(A + B)^2}{4} + C}, \quad (19)$$

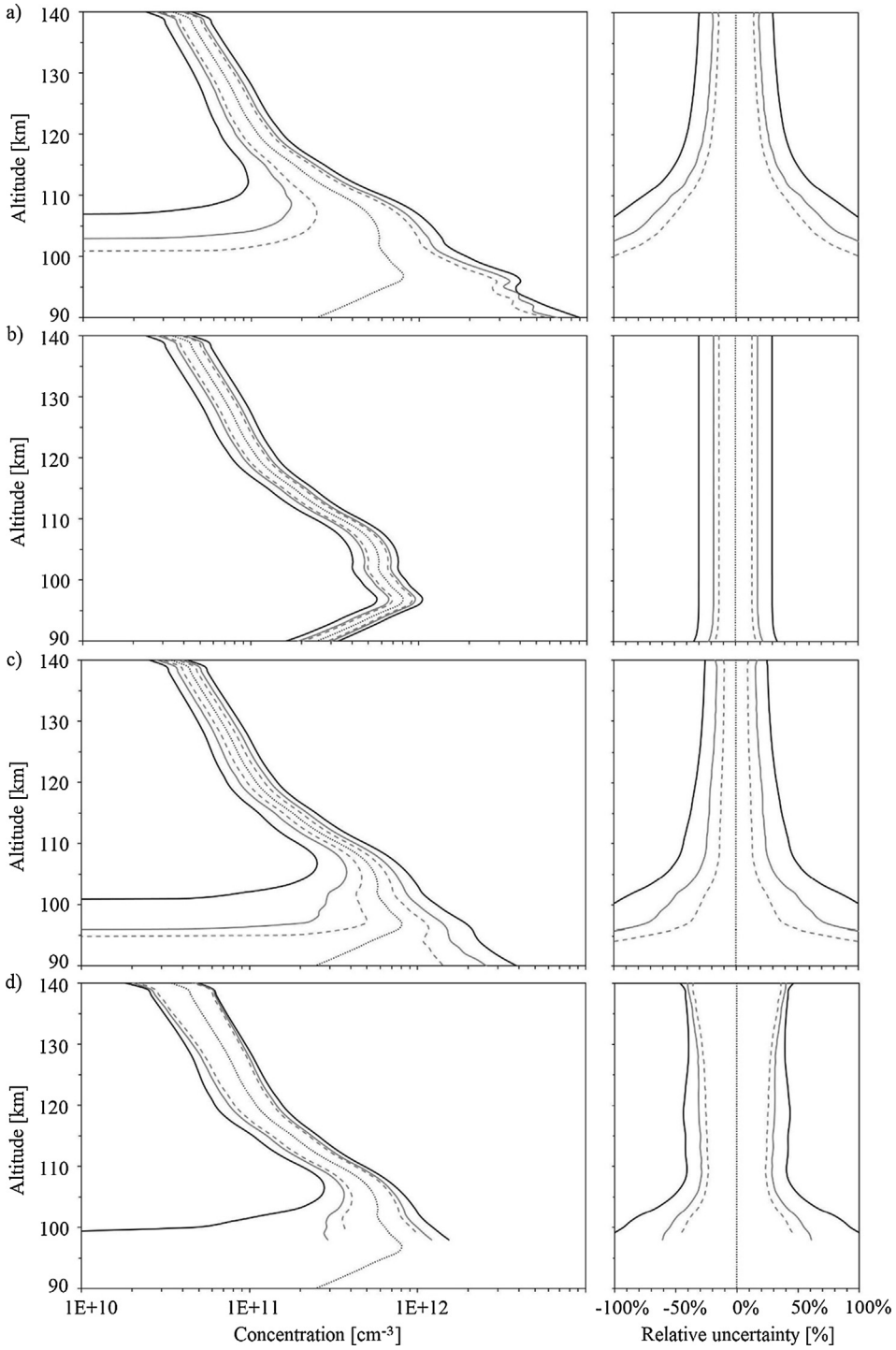

Fig. 4. Altitude dependence of the calculated relative uncertainty of the [$O(^3P)$] altitude profile retrieved from the next proxies: (a) $O(^1D)$, (b) $O_2(b^1\Sigma_g^+, v = 2)$, (c) $O_2(b^1\Sigma_g^+, v = 1)$, (d) $O_2(b^1\Sigma_g^+, v = 0)$. Left panel presents absolute uncertainty, right panel presents relative uncertainty. Legend: reference (black dotted line); results of the Monte Carlo simulation with the uniform (grey solid line) and the normal (grey dashed line) error distribution functions; results of the sensitivity analysis (black solid line).

where

$$A = \frac{[O_2]\cdot k(O(^1D);O_2) + [N_2]\cdot k(O(^1D);N_2) + [CO_2]\cdot k(O(^1D);CO_2)}{k(O(^1D);O(^3P))}$$

$$B = \frac{[O_2]\cdot g_\beta - [O_2(b,v=1)]\cdot\left(\tau^{-1}_{O_2(b,v=1)} + [O_2]\cdot k(O_2(b,v=1);O_2) + [CO_2]\cdot k(O_2(b,v=1);CO_2)\right)}{[O_2(b,v=1)]\cdot k(O_2(b,v=1);O(^3P))}$$

$$C = \frac{[O_2]\cdot k(O(^1D);O_2)\cdot\psi_1\cdot\left\{[O_2]\cdot\left(J_{SRC} + J_{Ly\alpha}\cdot F(Ly\alpha)\right) + [O_3]\cdot J_{HHB}\cdot F(HHB)\right\}}{[O_2(b,v=1)]\cdot k(O_2(b,v=1);O(^3P))\cdot k(O(^1D);O(^3P))}$$

Comparison of the results of statistical modeling by (19) is shown at Fig. 4c. As can be seen, the uncertainty of retrieval of $[O(^3P)]$ from $[O_2(b^1\Sigma_g^+,\ v=1)]$ does not exceed 20% above 110 km.

5.2.4. Retrieval of $[O(^3P)]$ from $[O_2(b^1\Sigma_g^+,\ v=0)]$

The ozone concentration decreases rapidly above 90 km, therefore the reaction $O_2(b^1\Sigma_g^+,\ v=0) + O_3 \rightarrow products$ can be discarded. Since rate coefficient of the reaction $O_2(b^1\Sigma_g^+,\ v=0) + O(^3P) \rightarrow products$ has large error (Supplementary Material), Kalogerakis (2019) assumed that this reaction can be neglected. Thus, we do not consider this reaction in (20). Moreover, the population of the level $O_2(b^1\Sigma_g^+,\ v=0)$ depends on the overlying levels $O(^1D)$ and $O_2(b^1\Sigma_g^+,\ v=1)$. Thus, we derived the analytical expression for retrieving $[O(^3P)]$ in the altitude range of 98–140 km:

$$[O(^3P)] = \frac{[O_2]\cdot k(O_2(b,v=1);O_2)}{k(O_2(b,v=1);O(^3P))}\cdot\frac{1-\Omega}{\Omega-\psi_0} - \frac{\tau^{-1}_{O_2(b,v=1)}}{k(O_2(b,v=1);O(^3P))}, \quad (20)$$

where

$$\Omega = \frac{[O_2(b,v=0)]\cdot\left(\tau^{-1}_{O_2(b,v=0)} + [N_2]\cdot k(O_2(b,v=0);N_2)\right) - [O_2]\cdot g_\alpha}{[O(^1D)]\cdot[O_2]\cdot k(O(^1D);O_2)}.$$

In the lower thermosphere, at the $O_2(b^1\Sigma_g^+,\ v=0)$ excitation the process of energy transfer from the excited atom $O(^1D)$ dominates in comparison with the population of this level by the absorption of solar radiation (g_α). In turn, processes characteristic of the ionosphere begin to contribute to the excitation of atoms $O(^1D)$ (electron–ion recombination, electron impact, etc.) (Witasse et al., 1999). Therefore, in order to retrieve $[O(^3P)]$, two parameters need to be taken into account in formula (20): $[O(^1D)]$ and $[O_2(b^1\Sigma_g^+,\ v=0)]$ which are derived from corresponding volume emission rates.

Fig. 4d presents a comparison of the simulation results. In this case, the uncertainty of $[O(^3P)]$ retrieval is greatly reduced from 60% to 30% in the altitude range of 98–105 km. Above 105 km, the uncertainty varies slightly with altitude and takes values from 25 to 40%.

5.3. Retrieval of the altitude profile of CO_2 concentration

In Yankovsky and Manuilova (2018) it was proved that $[CO_2]$ can be retrieved in the altitude range of 50–100 km using emissions of level $O_2(b^1\Sigma_g^+,\ v=0)$ as proxy. The remaining proxies, $O(^1D)$, $O_2(b^1\Sigma_g^+,\ v=2)$, $O_2(b^1\Sigma_g^+,\ v=1)$, $O_2(a^1\Delta_g,\ v=0)$, do not depend on $[CO_2]$. The sensitivity analysis showed that the uncertainty of $[CO_2]$ retrieval is within 15–30% in the altitude range of 50–85 km; above 85 km the sensitivity analysis of $[CO_2]$ retrieval was not performed. In this study, we conducted a research of the uncertainty of $[CO_2]$ retrieval in the extended altitude range of 50–100 km using Monte Carlo method.

In Yankovsky and Manuilova (2018), it was shown that the population of the level $O_2(b^1\Sigma_g^+,\ v=0)$ depends also on the overlying level $O_2(b^1\Sigma_g^+,\ v=1)$. Thus, the analytical expression for the volume mixing ratios of carbon dioxide, $C_{v,\ CO2}$, is:

$$C_{v,CO2} = \Omega_1 C_{v,O2}\frac{\omega_2[O_2(b,v=1)]\left\{k(O_2(b,v=1);O_2) + C_{v,O(3P)}k(O_2(b,v=1);O(^3P))/C_{v,O2}\right\} + g_\alpha}{[O_2(b,v=0)]} - \Omega_3 C_{v,N2} - \frac{\Omega_1\Omega_4 T}{p\tau_{O2(b,v=0)}} - \Omega_1 C_{v,O3}k(O_2(b,v=0);O_3) - \Omega_6 C_{v,O(3P)}, \quad (21)$$

where p is atmospheric pressure; the invariants which do not depend on altitude take values:

$$\omega_2 = \frac{1}{\psi_1} = 1.25,\ \Omega_1 = \frac{1}{k(O_2(b,v=0);CO_2)} = 2.27 \cdot 10^{12}\ \text{cm}^{-3}\ \text{s},$$
$$\Omega_3 = \frac{k\ (O_2(b,v\ =\ 0);\ N_2)}{k\ (O_2(b,v\ =\ 0);\ CO_2)} = 5 \cdot 10^{-3},$$
$$\Omega_4 = \frac{1}{7.24 \cdot 10^{18}} = 1.38 \cdot 10^{-19}\ \text{mb}\cdot\text{cm}^3\text{K}^{-1},$$
$$\Omega_6 = \frac{k\left(O_2(b,v\ =\ 0);O(^3P)\right)}{k(O_2(b,v\ =\ 0);CO_2)} = 0.182.$$

The values of invariants were estimated in Yankovsky and Manuilova (2018) using database of rate coefficients for reactions involving $O_2(b^1\Sigma_g^+,\ v = 0)$ and $O_2(b^1\Sigma_g^+,\ v = 1)$. Two measured parameters, $[O_2(b^1\Sigma_g^+,\ v = 0)]$ and $[O_2(b^1\Sigma_g^+,\ v = 1)]$, are needed to determine the volume mixing ratios of CO_2 in (21).

Fig. 5 displays a comparison of the uncertainty of $[CO_2]$ retrieval obtained by sensitivity analysis with the results obtained by the Monte Carlo method.

As can be seen from Fig. 5, estimation of the uncertainty of $[CO_2]$ retrieval below 85 km by the Monte Carlo method is about 10–25% and 7–17% for the uniform and normal error distribution of the parameters, respectively. Above 85 km, the uncertainty takes values of 25–70% and 18–53% for the uniform and normal error distribution of the parameters, respectively.

Based on the numerical experiment, it can be concluded that the $[CO_2]$ altitude profile can be retrieved in the altitude range of 50–100 km, but it should be borne in mind that above the mesopause region the magnitude of the uncertainty of carbon dioxide concentration is much larger.

6. Discussion

In the study the estimates of uncertainties for solving the forward and inverse problems by the Monte Carlo method are compared with the estimates obtained by the sensitivity analysis. Based on a comparison of the two approaches, it can be concluded that for all the considered forward (Section 4) and inverse (Section 5) problems, the relative uncertainties of solutions obtained by the Monte Carlo method are less than those obtained using the sensitivity analysis of the photochemical model. In our opinion, the Monte Carlo method provides more realistic estimates of the uncertainties, because it takes into account the random and independent change of each parameter in the limit of its error. Therefore, recommendations of methods for retrieving the concentrations of small gas components of the atmosphere from measurements of the intensity of oxygen emissions will be given, based on estimates obtained by the Monte Carlo method.

The dramatic increase of atomic oxygen concentration above 80 km in relation to the main components of the atmosphere, N_2 and O_2, affects the photochemistry and energetics of the mesosphere and lower thermosphere. Therefore, it is useful to consider the inverse problems in two regions (conditionally, below and above the mesopause region) independently.

More precisely the altitudes of the boundaries of the transition region are determined for each inverse problem in this study using the Monte Carlo method and sensitivity analysis (see Figs. 2–5).

As can be seen from Fig. 4, the altitude profile of atomic oxygen concentration can be retrieved only above about 90 km. The concentration profiles of ozone and carbon dioxide can be retrieved in two altitude intervals. The first interval is the range 50–85 km where the role of atomic oxygen is insignificant. For the second interval 85–100 km the $[O(^3P)]$, $[O_3]$ and $[CO_2]$ can be retrieved simultaneously if three different proxies are used (Figs. 3–5).

In most cases, the errors of the rate coefficients of reactions involving $O(^3P)$ are much larger than for collisional reactions involving N_2 and O_2. This leads to an increase in the uncertainty of the retrieved values of $[O_3]$ and $[CO_2]$ above mesopause region (see Sections 5.1.3, 5.1.4, 5.2.1, 5.2.3 and 5.3). Thus, improving the accuracy of measurements of the rate coefficients of collisional processes involving atomic oxygen is a task of great importance for decreasing the uncertainties of solutions of the inverse problems.

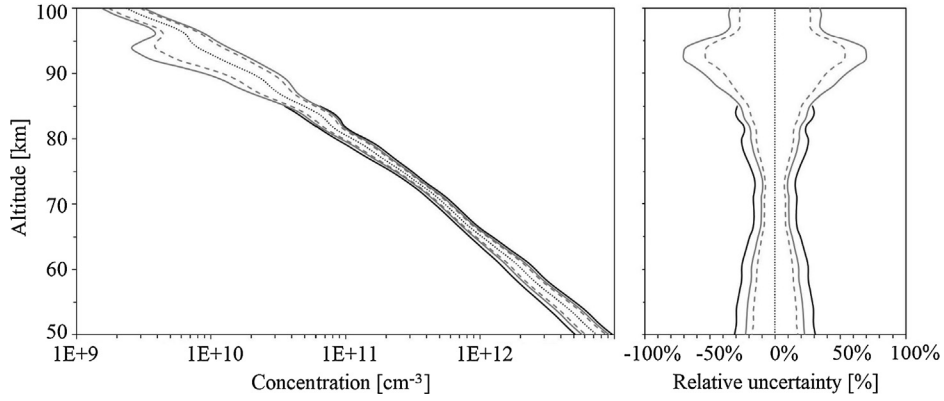

Fig. 5. Altitude dependence of the calculated relative uncertainty of the $[CO_2]$ altitude profile retrieved from proxies $O_2(b^1\Sigma_g^+, v = 0)$ and $O_2(b^1\Sigma_g^+, v = 1)$, see (21). Left panel presents absolute uncertainty, right panel presents relative uncertainty. Legend: reference (black dotted line); results of the Monte Carlo simulation with the uniform (grey solid line) and the normal (grey dashed line) error distribution functions; results of the sensitivity analysis (black solid line).

7. Conclusions

In the study, we present a complete summary of the methods for retrieving the altitude profiles of $[O(^3P)]$, $[O_3]$, and $[CO_2]$ in MLT from the measured volume emission rates of singlet electronically-vibrationally excited oxygen molecules $O_2(b^1\Sigma_g^+, v \le 2)$, $O_2(a^1\Delta_g, v = 0)$ and $O(^1D)$ atom as proxies of concentration of these components. For each of the proposed methods, we obtained an analytical expression linking the concentration of the target component to the concentration of proxy. The obtained results allow to retrieve the altitude profiles of $[O(^3P)]$, $[O_3]$, and $[CO_2]$ using:

(a) any of four methods (13–16) for O_3;
(b) any of four methods (17–20) for $O(^3P)$;
(c) method expressed by (21) for CO_2.

Some of the presented techniques for retrieving the concentration of target components were examined and verified in the previous publications (Yankovsky et al., 2016; Yankovsky and Manuilova, 2018), however, four methods have not previously been published. For the first time, two methods are presented for retrieving the $[O(^3P)]$ from the volume emission rates of excited molecular oxygen $O_2(b^1\Sigma_g^+, v = 2)$ and atomic oxygen $O(^1D)$. A new method for retrieving the $[O(^3P)]$ altitude profile from simultaneous observation of the volume emission rates of excited molecular oxygen $O_2(b^1\Sigma_g^+, v = 0)$ and atomic oxygen $O(^1D)$ is proposed, as well as a method for retrieving the $[O_3]$ from the volume emission rate of $O(^1D)$.

The relative uncertainties of forward and inverse problems were estimated using the Monte Carlo method for the uniform and normal distribution of the errors of the parameters of the model of photochemical kinetics of the O_2 and O_3 photolysis products in MLT, YM2011. In all the cases considered, we compared the results of numerical experiments using the Monte Carlo method and sensitivity analysis.

Based on the numerical experiments carried out in this paper, we recommend the following methods for retrieval of the $[O(^3P)]$ $[O_3]$ and $[CO_2]$ altitude profiles from measurements of the intensities of the oxygen emissions:

1. All the considered proxies are suitable for retrieving the $[O_3]$ altitude profile, but the optimal one is $[O_2(b^1\Sigma_g^+, v = 1)]$, which ensures a relative uncertainty of retrieval of about 6–12% in the altitude range of 50–96 km. Below 89 km, it is also possible to use the proxy $[O_2(a^1\Delta_g, v = 0)]$ with a relative uncertainty of the $[O_3]$ retrieval not exceeding 12%.
2. In the altitude range of 90–140 km, the use of the proxy $[O_2(b^1\Sigma_g^+, v = 2)]$ enables us to retrieve the $[O(^3P)]$ altitude profile with a relative uncertainty of about 18%. In the range of 105–140 km, it is also possible to use the simultaneous measurements of the concentrations $[O_2(b^1\Sigma_g^+, v = 0)]$ and $[O(^1D)]$ to retrieve $[O(^3P)]$ with the average relative uncertainty of about 25–40%.
3. To retrieve the $[CO_2]$ altitude profile we developed a method that uses the simultaneous measurement of the volume emission rates for the transitions from two excited levels of the oxygen molecule, $O_2(b^1\Sigma_g^+, v = 0)$ and $O_2(b^1\Sigma_g^+, v = 1)$. The proposed method allows to obtain the $[CO_2]$ altitude profile in the range of 50–85 km with an uncertainty of 10–20% and in the range of 85–100 km with an uncertainty of 20–60%.

Acknowledgments

Funding: This work was supported by the Russian Fund for Basic Research (grant RFBR No.17-05-00532). We thank anonymous referees for their valuable suggestions to improve the present study.

Author contributions

The author Yankovsky V. A. proposed the idea of the study, conducted a sensitivity analysis and derived the basic formulas, the author Vorobeva E. V. carried out all calculations connected with the Monte Carlo simulations. Analysis of results, the content of work, design, and manuscript preparation were joint efforts of all authors.

Declaration of Competing Interest

No competing interests are present.

Appendix A. *Oxygen Atmospheric and Noxon bands system transition arrays*

The Einstein coefficients $A_{v'v''}$ for the optical transitions are calculated by the formula (Kuznetsova et al., 1980; Kassi et al., 2005):

$$A_{v'v''} = A_{00}\frac{q_{v'v''}\nu^3_{v'v''}}{q_{00}\nu^3_{00}}, \quad \text{(A1)}$$

where $\nu_{v'v''}$ – transition energy in cm^{-1} (we used spectroscopic constants for $X^3\Sigma_g^-$ and $b^1\Sigma_g^+$ states from (Krupenie, 1972), and for $a^1\Delta_g$ state from (Slanger, 1978)), $q_{v'v''}$ – Franck- Condon factor for transition from the level with vibrational number v′ to the level with vibrational number v″ (Yu et al., 2014). In the formula (A1), the measured values of the Einstein coefficients for transitions from the level $v' = 0$ to the level $v'' = 0$ are used as the normalization factor A_{00}, namely, for Noxon band, $A_{O2(b,v'=0 \to a,\ v''=0)} = 1.5\cdot10^{-3}\ s^{-1}$ (Krupenie, 1972), for IR Atmospheric band, $A_{O2(a,v'=0 \to X,\ v''=0)} = 2.26\cdot10^{-4}\ s^{-1}$ (Newman et al., 2000). Currently, for Atmospheric band the range of experimentally measured values of A_{00} lies in the interval $0.077\ s^{-1}$ (Ritter and Wilkerson, 1987) to $0.0893\ s^{-1}$ (Schermaul and Learner, 1999), note, that the most recent result is $0.0874\ s^{-1}$ (Balasubramanian et al., 2014). Therefore, we use the traditional value $A_{O2(b,v'=0}$

Table A1
Einstein coefficients for probabilities of transitions from $O_2(b^1\Sigma_g^+, v')$ to $O_2(X^3\Sigma_g^-, v'')$ in the Atmospheric band.

v′	v″														
	0	1	2	3	4	5	6	7	8	9	10	11	12	13	14
0	8.50E-02	4.19E-03	1.04E-04	1.44E-06	1.37E-08	8.20E-11	2.30E-13	3.69E-15	2.07E-17						
1	8.28E-03	6.98E-02	8.04E-03	3.30E-04	6.74E-06	8.70E-08	6.95E-10	2.77E-12	3.43E-14	1.19E-16					
2	4.36E-04	1.58E-02	5.54E-02	1.14E-02	6.94E-04	1.95E-05	3.30E-07	3.42E-09	1.85E-11	1.89E-13	2.67E-16				
3	1.50E-05	1.39E-03	2.22E-02	4.20E-02	1.41E-02	1.20E-03	4.50E-05	9.71E-07	1.27E-08	9.02E-11	8.09E-13	1.40E-16			
4	2.76E-07	7.22E-05	2.91E-03	2.72E-02	3.00E-02	1.61E-02	1.85E-03	9.00E-05	2.44E-06	3.98E-08	3.61E-10	3.01E-12	4.55E-16		
5	8.92E-11	2.12E-06	2.14E-04	5.02E-03	3.05E-02	1.97E-02	1.71E-02	2.63E-03	1.63E-04	5.48E-06	1.10E-07	1.25E-09	1.03E-11	1.36E-14	
6	8.45E-10	1.10E-08	9.26E-06	5.00E-04	7.66E-03	3.19E-02	1.15E-02	1.72E-02	3.50E-03	2.73E-04	1.13E-05	2.76E-07	3.90E-09	3.28E-11	1.08E-13
7	2.01E-10	3.29E-09	1.35E-07	3.01E-05	1.00E-03	1.07E-02	3.14E-02	5.54E-03	1.64E-02	4.40E-03	4.31E-04	2.19E-05	6.45E-07	1.11E-08	1.00E-10
8	1.62E-11	1.40E-09	4.70E-09	8.36E-07	8.12E-05	1.81E-03	1.39E-02	2.91E-02	1.78E-03	1.46E-02	5.26E-03	6.45E-04	4.00E-05	1.42E-06	2.95E-08
9	4.29E-15	1.74E-10	5.05E-09	5.78E-10	3.59E-06	1.91E-04	3.00E-03	1.70E-02	2.51E-02	1.35E-04	1.21E-02	5.97E-03	9.20E-04	6.95E-05	2.94E-06
10	9.29E-13	3.09E-12	9.63E-10	1.19E-08	1.92E-08	1.22E-05	4.04E-04	4.62E-03	1.96E-02	1.99E-02	2.70E-04	9.21E-03	6.44E-03	1.25E-03	1.15E-04

Table A2
Einstein coefficients for probabilities of transitions from $O_2(b^1\Sigma_g^+, v')$ to $O_2(a^1\Delta_g, v'')$ in the Noxon band.

v′	v″														
	0	1	2	3	4	5	6	7	8	9	10	11	12	13	14
0	1.50E-03	1.30E-05	2.78E-08												
1	7.16E-05	1.36E-03	2.61E-05	9.03E-08											
2	2.06E-06	1.41E-04	1.23E-03	3.89E-05	1.95E-07										
3	4.23E-08	6.56E-06	2.08E-04	1.09E-03	5.15E-05	3.51E-07									
4	4.74E-10	1.98E-07	1.39E-05	2.70E-04	9.61E-04	6.36E-05	5.68E-07								
5	4.38E-14	3.51E-09	5.80E-07	2.44E-05	3.27E-04	8.34E-04	7.50E-05	8.55E-07							
6	9.84E-13	8.26E-12	1.52E-08	1.35E-06	3.84E-05	3.78E-04	7.12E-04	8.54E-05	1.23E-06						
7	6.00E-15	1.21E-12	1.57E-10	4.95E-08	2.73E-06	5.62E-05	4.21E-04	5.95E-04	9.47E-05	1.69E-06					
8	2.51E-13	4.13E-13	7.92E-13	1.12E-09	1.35E-07	5.03E-06	7.79E-05	4.55E-04	4.85E-04	1.03E-04	2.26E-06				
9	5.68E-13	3.77E-12	8.96E-12	4.93E-11	5.12E-09	3.26E-07	8.63E-06	1.04E-04	4.79E-04	3.83E-04	1.09E-04	2.94E-06			
10	6.55E-13	6.31E-12	2.64E-11	6.64E-11	4.03E-10	1.81E-08	7.11E-07	1.40E-05	1.33E-04	4.92E-04	2.90E-04	1.13E-04	3.74E-06		

Table A3
Einstein coefficients for probabilities of transitions from $O_2(a^1\Delta_g, v')$ to $O_2(X^3\Sigma_g^-, v'')$ in the IR Atmospheric band.

v′	v″														
	0	1	2	3	4	5	6	7	8	9	10	11	12	13	14
0	2.26E-04	1.53E-06	6.50E-09	5.14E-12	1.56E-14										
1	5.00E-06	2.13E-04	3.23E-06	2.19E-08	2.87E-11	9.51E-14									
2	4.03E-08	1.05E-05	2.00E-04	5.07E-06	4.94E-08	9.67E-11	3.63E-13								
3	5.16E-13	1.47E-07	1.64E-05	1.86E-04	7.04E-06	9.26E-08	2.54E-10	1.11E-12							
4	4.19E-11	3.92E-11	3.55E-07	2.26E-05	1.71E-04	9.11E-06	1.56E-07	5.75E-10	2.97E-12						
5	5.87E-12	1.80E-10	5.10E-10	7.04E-07	2.91E-05	1.56E-04	1.12E-05	2.44E-07	1.17E-09	7.17E-12					
6	5.61E-13	3.71E-11	4.63E-10	2.57E-09	1.24E-06	3.57E-05	1.40E-04	1.34E-05	3.64E-07	2.22E-09	1.60E-11				
7	8.23E-14	5.43E-12	1.39E-10	9.21E-10	8.68E-09	2.01E-06	4.23E-05	1.25E-04	1.54E-05	5.20E-07	3.95E-09	3.37E-11			
8	4.33E-14	1.22E-12	2.84E-11	4.01E-10	1.55E-09	2.32E-08	3.08E-06	4.87E-05	1.09E-04	1.74E-05	7.18E-07	6.73E-09	6.73E-11		
9	4.49E-14	6.40E-13	8.39E-12	1.08E-10	9.83E-10	2.27E-09	5.33E-08	4.49E-06	5.46E-05	9.30E-05	1.91E-05	9.65E-07	1.10E-08	1.28E-10	
10	4.45E-14	5.53E-13	4.55E-12	3.86E-11	3.31E-10	2.14E-09	2.95E-09	1.10E-07	6.30E-06	5.99E-05	7.78E-05	2.05E-05	1.26E-06	1.74E-08	2.34E-10

$\rightarrow X,\ v'' = 0) = 0.085\ s^{-1}$ (Krupenie, 1972). Tables A1–A3 presents Einstein coefficients for emission transitions from the upper to the lower levels.

Appendix B. Supplementary material

Supplementary data to this article can be found online at https://doi.org/10.1016/j.asr.2019.07.020.

References

Atkinson, R., Baulch, D.L., Cox, R.A., Crowley, J.N., Hampson, R.F., Hynes, R.G., Jenkin, M.E., Rossi, M.J., Troe, J., 2004. Evaluated kinetic and photochemical data for atmospheric chemistry: Volume I – gas phase reactions of O_x, HO_x, NO_x and SO_x species. Atmos. Chem. and Phys. 4 (6), 1461–1738. https://doi.org/10.5194/acp-4-1461-2004.

Balasubramanian, T.K., Mishra, A.P., Kshirsagar, R.J., 2014. Absorption intensities of rovibronic transitions in the A-band of $^{16}O_2$: Analysis and calculation of magnetic dipole and electric quadrupole contributions. J. Quant. Spectrosc. Radiat. Transfer 133, 91–98. https://doi.org/10.1016/j.jqsrt.2013.07.018.

Burkholder, J.B., Abbatt, J.P.D., Huie, R.E., Kurylo, M.J., Wilmouth, D. M., Sander, S.P., Barker, J.R., Kolb, C.E., Orkin, V.L., Wine, P.H., 2015. Chemical Kinetics and Photochemical Data for Use in Atmospheric Studies, JPL Publication 15–10, Evaluation Number 18. California Institute of Technology, Pasadena, California, http://hdl.handle.net/2014/45510.

Burrows, S.M., Rayner, P.J., Butler, T., Lawrence, M.G., 2013. Impact of modelled particle characteristics on emissions inferred by inversion of tracer transport. Atmos. Chem. Phys. Discussion 13, 4391–4432. https://doi.org/10.5194/acpd-13-4391-2013.

Christensen, A.B., Yee, J.-H., Bishop, R.L., Budzien, S.A., Hecht, J.H., Sivjee, G., Stephan, A.W., 2012. Observations of molecular oxygen Atmospheric band emission in the thermosphere using the near infrared spectrometer on the ISS/RAIDS experiment. J. Geophys. Res. 117, A04315. https://doi.org/10.1029/2011JA016838.

Evans, W.F.J., McDade, I.C., Yuen, J., Llewellyn, E.J., 1988. A rocket measurement of the O_2 Infrared Atmospheric (0–0) band emission in the dayglow and a determination of the mesospheric ozone and atomic oxygen densities. Can. J. Phys. 66 (11), 941–946. https://doi.org/10.1139/p88-151.

Forsythe, G.E., Malcolm, M.A., Moler, C.B., 1977. Computer methods for mathematical computations, ed. Prentice-Hall, Englewood Cliffs, N.J., https://books.google.ru/books?id=FvdQAAAAMAAJ.

Gamache, R.R., Goldman, A., 2001. Einstein A coefficient, integrated band intensity, and population factors: application to the $a^1\Delta_g - X^3\Sigma_g^-$ (0, 0) O_2 band. J. Quant. Spectrosc. Radiat. Transfer 69 (4), 389–401. https://doi.org/10.1016/S0022-4073(00)00072-8.

Gao, F.-L., Tao, L.-R., Cui, G.-M., Xu, J.-L., Hua, T.-C., 2015. The influence of solar spectral variations on global radiative balance. Adv. Space Res. 55, 682–687. https://doi.org/10.1016/j.asr.2014.10.028.

Gattinger, R.L., McDade, I.C., Alfaro Suzan, A.L., Boone, C.D., Walker, K.A., Bernath, P.F., Evans, W.F.J., Degenstein, D.A., Yee, J.-H., Sheese, P., Llewellyn, E.J., 2010. NO_2 air afterglow and O and NO densities from Odin-OSIRIS night and ACE-FTS sunset observations in the Antarctic MLT region. J. Geophys. Res. 115, D12301. https://doi.org/10.1029/2009JD013205.

Grygalashvyly, M., Eberhart, M., Hedin, J., Strelnikov, B., Lübken, F.-J., Rapp, M., Löhle, S., Fasoulas, S., Khaplanov, M., Gumbel, J., Vorobeva, E., 2019. Atmospheric band fitting coefficients derived from a self-consistent rocket-borne experiment. Atmos. Chem. Phys. 19, 1207–1220. https://doi.org/10.5194/acp-19-1207-2019.

Hecht, J.H., Christensen, A.B., Yee, J.-H., Crowley, G., Bishop, R.L., Budzien, S.A., Stephan, A.W., Evans, J.S., 2015. A new technique for remote sensing of O_2 density from 140 to 180 km. Geophys. Res. Lett. 42, 233–240. https://doi.org/10.1002/2014GL062355.

Hedin, J., Gumbel, J., Stegman, J., Witt, G., 2009. Use of O_2 airglow for calibrating direct atomic oxygen measurements from sounding rockets. Atmos. Meas. Tech. 2, 801–812. https://doi.org/10.5194/amt-2-801-2009.

Jonsson, A.I., 2006. Modelling the middle atmosphere and its sensitivity to climate change. Doctoral thesis. Department meteorology, Stockholm University. ISBN 91-7155-185-9, pp. 1–30. https://www.cetesb.sp.gov.br/proclima/wp-content/uploads/sites/36/2014/05/jonsson_modelling_middle.pdf.

Kalogerakis, K.S., 2019. A previously unrecognized source of the O_2 Atmospheric band emission in Earth's nightglow. Sci. Adv. 5, eaau9255.

Kassi, S., Romanini, D., Campargue, A., Bussery-Honvault, B., 2005. Very high sensitivity CW-cavity ring down spectroscopy: Application to the $a^1\Delta_g(0) - X^3\Sigma_g^-(1)$ O_2 band near 1.58 μm. Chem. Phys. Lett. 409, 281–287. https://doi.org/10.1016/j.cplett.2005.05.033.

Khabibrakhmanov, I.K., Degenstein, D.A., Llewellyn, E.J., 2002. Mesospheric ozone: Determination from orbit with the OSIRIS instrument on ODIN. Can. J. Phys. 80 (4), 493–504. https://doi.org/10.1139/p02-022.

Krupenie, P.H., 1972. The spectrum of molecular oxygen. J. Phys. Chem. Ref. Data 1 (2), 423–521. https://doi.org/10.1063/1.3253101.

Kuznetsova, L.A., Kuzmenko, N.E., Kuziakov, Iu. Ia., Plastinin, Iu. A., 1980. Probabilities of optical transitions of diatomic molecules (in Russian), ed. NAUKA, Moscow.

Llewellyn, E.J., Witt, G., 1977. The measurement of ozone concentrations at high latitude during the twilight. Planet. Space Sci. 25, 165–172. https://doi.org/10.1016/0032-0633(77)90021-6.

Marsh, D.R., Skinner, W.R., Marshall, A.R., Hays, P.B., Ortland, D.A., Yee, J.-H., 2002. High resolution doppler imager observations of ozone in the mesosphere and lower thermosphere. J. Geophys. Res. 107 (D19), 4390. https://doi.org/10.1029/2001JD001505.

Martyshenko, K.V., Yankovsky, V.A., 2017. IR band of O_2 at 1.27 μm as the tracer of O_3 in the mesosphere and lower thermosphere: correction of the method. Geomag. Aeron. 57 (2), 229–241. https://doi.org/10.1134/S0016793217020098.

Mlynczak, M.G., Morgan, F., Yee, J.-H., Espy, P., Murtagh, D., Marshall, B.T., Schmidlin, F., 2001. Simultaneous measurements of the $O_2(a^1\Delta_g)$ and $O_2(b^1\Sigma_g^+)$ airglows and ozone in the daytime mesosphere. Geophys. Res. Lett. 28 (6), 999–1002. https://doi.org/10.1029/2000GL012423.

Mlynczak, M.G., Solomon, S.C., Zaras, D.S., 1993. An updated model for $O_2(a^1\Delta_g)$ concentrations in the mesosphere and lower mesosphere and implications for remote sensing of ozone at 1.27 μm. J. Geophys. Res. 98 (D10), 18639–18648. https://doi.org/10.1029/93JD01478.

Newman, S.M., Orr-Ewing, A.J., Newnham, D.A., Ballard, J., 2000. Temperature and pressure dependence of line widths and integrated absorption intensities of the $O_2(a^1\Delta_g - X^3\Sigma_g^-(0, 0))$. J. Phys. Chem. A 104 (42), 9467–9480. https://doi.org/10.1021/jp001640r.

Pejakovic, D.A., Copeland, R.A., Slanger, T.G., Kalogerakis, K.S., 2014. $O_2(b^1\Sigma_g^+, v = 0, 1)$ relative yields in $O(^1D) + O_2$ energy transfer 024303. J. Chem. Phys. 141. https://doi.org/10.1063/1.4885721.

Picone, J.M., Hedin, A.E., Drob, D.P., Aikin, A.C., 2002. NRLMSISE-00 empirical model of the atmosphere: Statistical comparisons and scientific issues. J. Geophys. Res. 107 (A12), 1468. https://doi.org/10.1029/2002JA009430.

Rezac, L., Kutepov, A., Russell III, J.M., Feofilov, A.G., Yue, J., Goldberg, R.A., 2015. Simultaneous retrieval of T(p) and CO_2 VMR from two-channel non-LTE limb radiances and application to daytime SABER/TIMED measurements. J. Atmos. Sol.-Terrestrial Phys. 130–131, 23–42. https://doi.org/10.1016/j.jastp.2015.05.004.

Ritter, K.J., Wilkerson, T.D., 1987. High-resolution spectroscopy of the oxygen A band. J. Mol. Spectrosc. 121, 1–19. https://doi.org/10.1016/0022-2852(87)90167-6.

Schermaul, R., Learner, R.C.M., 1999. Precise line parameters and transition probability of the atmospheric A band of molecular oxygen $^{16}O_2$. J. Quant. Spectrosc. Radiat. Transfer 61, 781–794. https://doi.org/10.1016/S0022-4073(98)00066-1.

Shmakov, A.V., Ustinov, E.A., 1994. Determination of the mesospheric ozone using satellite limb-scan measurements of the infra-red atmospheric band emission of $O_2(a^1\Delta_g)$. J. Atmos. Terrestrial Phys. 56 (9), 1083–1090. https://doi.org/10.1016/0021-9169(94)90046-9.

Simeckova, M., Jacquemart, D., Rothman, L.S., Gamache, R.R., Goldman, A., 2006. Einstein A-coefficients and statistical weights for molecular absorption transitions in the HITRAN database. J. Quant. Spectrosc. Radiat. Transfer 98, 130–155. https://doi.org/10.1016/j.jqsrt.2005.07.003.

Slanger, T.G., 1978. Generation of $O_2(c^1\Sigma_u^-, C^3\Delta_u, A^3\Sigma_u^+)$ from oxygen atom recombination. J. Chem. Phys. 69 (11), 4779–4791. https://doi.org/10.1063/1.436504.

Slanger, T.G., Copeland, R.A., 2003. Energetic oxygen in the upper atmosphere and the laboratory. Chem. Rev. 103 (12), 4731–4766. https://doi.org/10.1021/cr0205311.

Slanger, T.G., Pejakovic, D.A., Kostko, O., Matsiev, D., Kalogerakis, K. S., 2017. Atmospheric dayglow diagnostics involving the O_2(b-X) Atmospheric band emission: Global Oxygen and Temperature (GOAT) mapping. J. Geophys. Res. Space Phys. 122 (3), 3640–3649. https://doi.org/10.1002/2016JA023502.

Smith, A.K., Harvey, V.L., Mlynczak, M.G., Funke, B., Garcia-Comas, M., Kaufmann, M., Kyrölä, E., López-Puertas, M., McDade, I., Randall, C.E., Russell III, J.M., Sheese, P.E., Shiotani, M., Skinner, W.R., Suzuki, M., Walker, K.A., 2013. Satellite observations of ozone in the upper mesosphere. J. Geophys. Res. 118, 5803–5821. https://doi.org/10.1002/jgrd.50445.

SORCE - Solar Radiation and Climate Experiment NASA Science Mission, 2003. http://science.nasa.gov/missions/sorce/.

Torr, M.T., Torr, D.G., 1985. A preliminary spectroscopic assessment of the spacelab 1/shuttle optical environment. J. Geophys. Res. 90 (A2), 1683–1690. https://doi.org/10.1029/JA090iA02p01683.

von Savigny, C., McDade, I.C., Griffioen, E., Haley, C.S., Sioris, C.E., Llewellyn, E.J., 2005. Sensitivity studies and first validation of stratospheric ozone profile retrievals from Odin/OSIRIS observations of limb-scattered solar radiation. Can. J. Phys. 83, 957–972. https://doi.org/10.1139/P05-041.

Vorobeva, E., Yankovsky, V., Schayer, V., 2018. Estimation of uncertainties of the results of [O(3P)], [O3] and [CO2] retrievals in the mesosphere according to the YM2011 model by two approaches: sensitivity study and Monte Carlo method. Poster EGU2018-17950. EGU General Assembly, April 8-13, 2018. Vienna, Austria. https://presentations.copernicus.org/EGU2018-17950_presentation.pdf.

Witasse, O., Lilensten, J., Lathuillare, C., Blelly, P.-L., 1999. Modeling the OI 630.0 and 557.7 nm thermospheric dayglow during EISCAT-WINDII coordinated measurements. J. Geophys. Res. 104 (A11), 24639–24655. https://doi.org/10.1029/1999JA900260.

Wu, K., Fu, D., Feng, Y., Li, J., Hao, X., Li, F., 2018. Simulation and application of the emission line $O_{19}P_{18}$ of $O_2(a^1\Delta_g)$ dayglow near 1.27 μm for wind observations from limb-viewing satellites. Opt. Express 26 (13), 16984–16999. https://doi.org/10.1364/OE.26.016984.

Yankovsky, V.A., Babaev, A.S., 2011. Photolysis of O_3 at hartley, chappuis, huggins, and wulf bands in the middle atmosphere: vibrational kinetics of oxygen molecules $O_2(X^3\Sigma_g^-, v\leq35)$. Atmos. Ocean. Opt. 24, 6–16. https://doi.org/10.1134/S1024856011010155.

Yankovsky, V.A., Kuleshova, V.A., Manuilova, R.O., Semenov, A.O., 2007. Retrieval of total ozone in the mesosphere with a new model of electronic-vibrational kinetics of O_2 and O_3 photolysis products. Izvestiya, Atmos. Ocean. Phys. 43 (4), 514–525. https://doi.org/10.1134/S0001433807040135.

Yankovsky, V.A., Manuilova, R.O., 2006. Model of daytime emissions of electronically-vibrationally excited products of O_3 and O_2 photolysis: application to ozone retrieval. Ann. Geophys. 24 (11), 2823–2839. https://doi.org/10.5194/angeo-24-2823-2006.

Yankovsky, V.A., Manuilova, R.O., 2018. Possibility of simultaneous [O_3] and [CO_2] altitude distribution retrievals from the daytime emissions of electronically-vibrationally excited molecular oxygen in the mesosphere. J. Atmosp. Solar-Terrest. Phys. 179, 22–33. https://doi.org/10.1016/j.jastp.2018.06.008.

Yankovsky, V.A., Manuilova, R.O., Babaev, A.S., Feofilov, A.G., Kutepov, A.A., 2011. Model of electronic-vibrational kinetics of the O_3 and O_2 photolysis products in the middle atmosphere: applications to water vapor retrievals from SABER/TIMED 6.3 μm radiance measurements. Int. J. Remote Sensing 32, 3065–3078. https://doi.org/10.1080/01431161.2010.541506.

Yankovsky, V.A., Martyshenko, K.V., Manuilova, R.O., Feofilov, A.G., 2016. Oxygen dayglow emissions as proxies for atomic oxygen and ozone in the mesosphere and lower thermosphere. J. Molec. Spectrosc. 327, 209–232. https://doi.org/10.1016/j.jms.2016.03.006.

Yee, J.-H., DeMajistre, R., Morgan, F., 2012. The $O_2(b^1\Sigma_g^+)$ dayglow emissions: application to middle and upper atmosphere remote sensing. Can. J. Phys. 90, 769–784. https://doi.org/10.1139/p2012-073.

Yu, S., Drouin, B.J., Miller, C.E., 2014. High resolution spectral analysis of oxygen. IV. Energy levels, partition sums, band constants, RKR potentials, Franck-Condon factors involving the $X^3\Sigma_g^-$, $a^1\Delta_g$ and $b^1\Sigma_g^+$ states. J. Chem. Phys. 141. https://doi.org/10.1063/1.4900510.